N71-33785
NASA TM X-67904

NASA TECHNICAL MEMORANDUM

NASA TM X-67904

PRELIMINARY TEST RESULTS OF HEAT TRANSFER/THERMAL STORAGE TUBE DESIGN UNDER SIMULATED ORBITAL CONDITIONS

by David Namkoong
Lewis Research Center
Cleveland, Ohio
August 1971

This information is being published in preliminary form in order to expedite its early release.

ABSTRACT

Heat-receiver tubes were tested as part of an investigation of a heat receiver for a solar Brayton-cycle power system. The tubes were designed to store excess solar energy during the orbital sunlit period and then to transfer the heat energy to the flowing gas during the orbital shade period. In this way constant thermal input to the Brayton system would be maintained over the entire orbit. The tubes utilized the heat of fusion of lithium fluoride as the heat-storage medium and were designed to accommodate the 23-percent volume change of LiF during phase changes.

The columbium-1% zirconium tubes operated under a simulated orbital condition for 2002 hours and 1251 sun-shade cycles before going into a scheduled shutdown. Although there were no gross distortions of the convoluted LiF-storage tubes, local distortions were detected. During operation, the gas discharge temperature varied from 30° below nominal at the end of the shade period to 50° above at the end of sunlit period. Surface temperatures along the tube ranged from 1410° F to 1670° F.

E-6511

PRELIMINARY TEST RESULTS OF HEAT TRANSFER/THERMAL STORAGE TUBE DESIGN UNDER SIMULATED ORBITAL CONDITIONS

by

David Namkoong

Lewis Research Center

SUMMARY

The effective use of a space power system based on the Brayton cycle with solar heating is highly dependent upon the performance of the solar-heat receiver. This receiver must store excess solar energy during the sunlit period and then transfer this stored energy to the Brayton system during shade time in order to maintain constant thermal input over the entire orbit. In the receiver design, the thermal storage and heat transfer to the Brayton-cycle working fluid (gas) is accomplished by the use of coaxial tubes with gas flowing in the inner tube, lithium fluoride located in the annulus and with incoming heat transmitted through the outer tube. The tubes were designed to operate under gravity conditions ranging from 0- to 1-g. The outer (coaxial) tube was bellows-shaped (convoluted) so that the thermal-storage salt would be distributed along the flow length in nearly self-contained units. Both tubes were made from columbium-1% zirconium.

As part of the development of the full receiver, tests were conducted on three receiver tubes under conditions simulating a near-Earth orbital mission; i.e., within a vacuum chamber and with radiant heaters on a 60-minutes-on, 36-minutes-off continuous cycle. The initial test was conducted with a high-solar-absorptivity coating, Fe_2TiO_5, on the outside surface of the convoluted tube. After 150 hours of testing, the coating was found to have decomposed, and the base metal to be contaminated with oxygen from the coating. In the second phase of testing, no coating was used; instead, the bare columbium-1% zirconium tube surface was grit-blasted to increase its solar absorptivity. Results showed that the grit-blasted approach provided a stable surface with adequate solar absorptivity.

Testing proceeded for 2002 hours and 1251 sun-shade cycles before terminating in a scheduled shutdown. Post-test inspection revealed no gross distortions, but local distortions did

occur in individual convolutions (bellows) in the gas-inlet region. Measured temperatures along the tube ranged from 1410° F to 1670° F. In addition, the temperature at each tube-surface location varied during a typical sun-shade cycle. This variation in tube temperature was at least partly reflected in the gas discharge temperature. The gas varied from 30° below to 50° above the nominal value of 1500° F and was repeatable for the 1251 cycles. This variation was within the design goal of receiver performance.

INTRODUCTION

In space, electric power can be generated by the conversion of solar heat. If a solar-heated powerplant is in Earth orbit however, there will be portions of the orbit during which the powerplant is in the Earth's shadow. Any design of such a powerplant in an orbiting craft must therefore consider the storage of thermal energy for use during the shadow period. One system that could be considered for an orbital mission and that could utilize solar energy is based on the Brayton cycle. The Brayton cycle, shown schematically in figure 1, employs a dynamic power system in which the working fluid gains energy from an outside source (such as from the Sun) and usefully converts it to electrical energy through the turbomachinery.

At the present time, a Brayton-cycle system is being investigated by the Lewis Research Center primarily for use with an isotope heat source. This same system, however, could be used with solar heating as well. To provide for this solar-heating option, a solar-heat receiver has been designed and fabricated. A photograph of the actual solar-heat receiver is shown in figure 2.

The thermal storage and heat transfer to the working fluid, a gaseous mixture of helium and xenon, are accomplished by the use of 48 coaxial pairs of tubes. Gas flows through the inner tube, and lithium fluoride is confined within the annular volume (see figure 3). During the sunlit period of the orbit, part of the heat transferred through the outer-tube surface is transferred to the flowing gas. The remainder liquefies the solid salt. During the shadow period, the liquid LiF solidifies, giving up its latent heat to the gas. In this way, the gas-discharge temperature is expected to stay essentially constant throughout the entire orbit.

A prime concern in the design of the tubes was that of controlling the distribution of the LiF. In changing from a liquid to a solid phase, the LiF undergoes a 23-percent decrease in volume. Without due consideration for this shrinkage, the void volume could be distributed adversely and cause

inadequate heating of the gas. Without LiF in contact with the tube surface in order to absorb some of the solar energy incident on that region, the outer-tube surface could overheat during the sunlit period. The requirement that the tubes must be able to operate under 1-g as well as 0-g further aggravates the LiF distribution problem.

The design upon which the tubes were built calls for a convoluted outer tube, the neck of which is within 0.030 inch of the inner tube. At the onset of freezing, the clearance between the tubes is expected to be plugged with solid LiF, sealing the remaining LiF within each convolution. In this way, LiF would remain properly distributed along the active heat-transfer length of the tube during melting and freezing, under either 1- or 0-g.

The inner tube is $1\frac{1}{4}$ inches in diameter with circumferential grooves rolled at 1-inch intervals. The grooves serve to increase the gas-side convective heat-transfer coefficient to that value required to attain the design discharge temperature.

Columbium-1% zirconium (Nb-1Zr) was used for the tube material as well as being used throughout the heat receiver. The high conductivity, the low elastic modulus, the low coefficient of thermal expansion, and the temperature tolerance of this refractory, allow latitude in designing for extended structural life at the expected elevated temperature levels.

The heat-flux distribution absorbed by the convoluted tube depends upon the absorptive and emissive properties of the surface. Since the gas-side capability was designed on the basis of a heat flux distribution close to that of the incident solar flux, a high value of solar absorptivity was deemed necessary. An analysis described in reference 1 confirms the importance of surface absorptivity within the receiver. To obtain a high value, the tubes were coated with iron titanate. To obtain a high value without coating, another set of tubes was grit blasted. Both types of surfaces were tested.

In this investigation, the heat-transfer/storage-tube design was evaluated in terms of its impact on the performance of the total receiver. As such, the following items were deemed as key areas of concern:

1. Heat transfer to and pressure drop of the gas.

2. Variation in gas-outlet temperature during the orbital period.

3. Localization of the LiF. Do the convolutions adequately prevent longitudinal migration of the LiF, or is the migration so serious that thermal performance is impaired?

4. Mechanical integrity of the tubes. Do the convolutions distort or fail in fatigue under the thermal cycling imposed by successions of sun-shade operation?

5. Stability of iron titanate in this application.

A complete thermal analysis of the solar-receiver tubes that adequately evaluates its performance presents a formidable task. Any study or experimental investigation that has been undertaken thus far on a thermal storage design has been based on relatively simple geometries, most noteworthy being those of R. A. McKinnon (ref. 2, 3, 4). The configurations studied included the salt (LiF or LiH) between two thick plates with and without fins, and also included tubes containing flowing gas, immersed in a bath of salt.

The present design, consisting of a convoluted geometry, renders heat-transfer analysis most difficult. This is apparent when one considers such factors within a single convolution as the continually varying phase percentage of the salt during the sun-shade cycle, void formation and distribution as the salt solidifies, and thermal radiation between the given convolution and the total receiver. These factors all affect the heat transfer from a convolution to the gas and, cumulatively, affect the gas-discharge temperature. These factors also determine the thermal stresses on the convolutions.

Because of the complexity of analysis, it was decided to evaluate the receiver tube design experimentally by subjecting three such tubes to conditions simulating an orbital mission. A configuration of three tubes, side-by-side, was chosen with the two outside tubes used as guards to provide the correct thermal environment for the center tube. In this way, the middle tube would experience the same radiation interchange with the adjacent tubes as in the receiver. The tubes were tested in a vacuum chamber and exposed to an electrically powered radiant heater. In simulation of a low-altitude orbit, the heat-input rate was applied periodically, 60 minutes on and 36 minutes off. Test time under these simulated conditions totalled 2002 hours. Helium-xenon was circulated through the tubes under conditions simulating operation in the Brayton power system. Surface temperatures on the tubes, gas temperatures entering and leaving the tubes, and pressure drop through the tubes were measured.

This report evaluates the heat-transfer/storage tube design by presenting the performance and post-test examination of the 2002-hour test of these three tubes.

APPARATUS

Test Section

The three receiver tubes were mounted within one-half of a water-cooled copper box as shown in figure 4. Tantalum heaters to simulate the solar flux to the tubes were mounted within the mating half of the box as shown in figure 5. The relative position between the tubes and the heaters within the closed box is illustrated in figure 6. Columbium and molybdenum sheets functioned as radiation shields between the interior and the copper box.

The three columbium-1% zirconium receiver tubes are of identical design - a 37-convolute tube fitted coaxially over a 1¼-inch diameter tube. The convoluted tube is made up of discs formed into half convolution shapes and electron-beam welded together. Dimensions are indicated in figure 7 and table I. The volume between the tubes was filled with molten lithium fluoride at a fill temperature of 1750° F. This temperature is 190° above the salt's melting temperature. It is also about 90° above the hottest temperature at which the receiver is expected to operate; thus providing additional volume for thermal expansion. A radial clearance of 0.015 inch is provided between the neck of the convolutions and the inside tube to allow for transfer of the molten salt from one convolution to the next during the filling operation. This small annulus, as mentioned previously, enables a frozen LiF barrier to be formed readily during an orbital mission thereby maintaining the proper distribution of salt along the tube. The convolution volume varies along the length of the tube in proportion to the solar heat flux impinging upon it. The inside tube through which the gas flows is grooved circumferentially every inch for 36 inches. These grooves function as turbulators to increase gas side-heat transfer.

In the initial performance tests, the outer surface of the convolutions was coated with plasma-sprayed iron titanate (Fe_2TiO_5). For the endurance test, no coating was used. Instead, the outer surface was grit-blasted with 250-micron Al_2O_3 particles. In both cases the intent was to produce a high solar-absorptive, emissive surface. Reference 1 discusses the influence of a range of these radiation properties and concludes that while both are important to receiver performance, solar absorptivity is primarily so. Though the iron titanate coating

indicated higher absorptance values and therefore was more desirable, there was a metallurgical and physical breakdown of the coating during the initial test. This result precipitated the decision to switch to the grit-blasted tubes. The coating breakdown is described in detail in a later section of this report.

Heaters within the test section fall into two classifications - the primary heater which basically provides the distribution of the solar heat flux, and the guard heater which is used to eliminate heat loss from the back side of the primary heater. Two radiation shields separate the primary heater from the guard. The primary heater is divided into fifteen zones ranging in length from 2 inches to 4 inches along the tube axis. The guard heater is divided into 4 zones ranging from 8 to 12 inches along the axial length. Each zone in both the primary and guard heaters is separately controlled.

Radiation shielding in the form of four thin sheets (innermost sheet columbium, the outer three, molybdenum) was installed on all interior surfaces of the copper box except for the area behind the tubes. Here, 20 thin columbium sheets, held apart by surface dimples were installed for the initial test. For the endurance phase of testing, a 60-layer, compact, multifoil heat shield (20 layers molybdenum, 40 layers nickel) was added behind the tubes. The additional insulation served to reduce heat loss further.

Test Facilities

The facility used for testing the three receiver tubes featured a vacuum tank that housed the test section and maintained pressure in the 10^{-8} torr range.

The closed gas system is shown as a schematic in figure 8. In operation, a diaphragm compressor was the driving force to circulate the gas around the loop. A bypass line was incorporated to control the flow rate to the test section. The discharge gas from the compressor was passed through a water-cooled heat exchanger so that its flow rate could be measured at a constant temperature. Because diaphragm compressors are known to operate with a significant amount of pressure oscillation, surge tanks were installed on both the upstream side of the compressor and the downstream side to minimize this effect. The pressure oscillations during the test were damped from approximately ± 10 psi at the compressor to $\pm \frac{1}{4}$ psi at the test section. Gas flow rate was measured before the flow was divided as well as in each of the three lines. Flow rate was controlled by a valve in each line. A finned heater rod functioning as a preheater heated

the flowing gas from room temperature to approximately 1200° F. A trim heater further downstream served to provide fine control of gas inlet temperature to each tube.

The gas then passed through the test section oriented so that the tubes were 21½° from the vertical, the same angle as the tubes in the receiver with the receiver axis vertical. This can be seen in figure 9 taken with the lid and cold wall removed from the vacuum tank. From the test section, the three lines merge, pass through the vacuum tank wall and into two water-cooled heat exchangers. The throttle valve serves to control the pressure level within the test section. Cooled to room temperature, the gas returns to the compressor to be recirculated.

Bimetallic joints were used to provide the tube-to-tube connection between the stainless steel and the columbium. These joints were of tongue-in-groove brazed design as shown in figure 10 and used at the inlet and discharge for each of the three receiver tubes.

INSTRUMENTATION

Temperatures on the columbium receiver tubes and backing sheet were measured by calibrated platinum/platinum 13% rhodium, 24-gage thermocouples connected to two 24-channel Brown recorders. The calibration tests showed results well within NASA CURE Specification U-50 and approaching limits of error for ISA special-grade wire. A post-test recalibration was conducted on a thermocouple that was attached to tube No. 2 in the high-heat flux region. With an immersion of 6 inches in the reference oven, the thermocouple indicated 0.7° higher and 1.4° lower than reference temperatures at 1240° F and 1792° F respectively. These differences are well within the limits of Specification U-50. Within the test section, all Pt/Pt13Rh thermocouples had a minimum of 6 inches exposed to near-isothermal surroundings.

The same type of thermocouple was attached to the two shields between the primary and guard heaters and connected to indicators. Those temperatures that were not expected to exceed 200° F (usually associated with water-cooled components) were measured by means of iron-constantan thermocouples. The remaining thermocouples were chromel-alumel. Both the iron-constantan and chromel-alumel wires met the ISA specifications.

Of special interest regarding thermocouple use is the temperature measurement of the gas into and out of the receiver tubes. To measure the bulk gas temperature, each thermocouple was incorporated into a flow mixer. The mixer was designed to force the gas to flow turbulently in continually changing directions so that the thermocouples would be measuring a true

averaged gas temperature. Initially, the flow mixer was separated from the receiver tube by a 90° elbow and a columbium-1% zirconium/stainless steel transition joint. Tests with this original scheme indicated excessive heat loss taking place between the receiver tubes and the mixers. For the endurance test, a new flow-mixing section was designed to be positioned close to the active length of the receiver tube. This design is shown in figure 11. Because it was designed to fit inside the 1¼-inch tube, this section was positioned to within 1 inch of the last convolution of the tube. This design features both outside and internal radiation shields to minimize heat loss or heat addition to the mixed gas. The inlet gas temperature was measured in the same manner.

He-Xe pressures throughout the system were measured by Bourdon tube gages. Where accurate readings were required, such as at the receiver tube inlet and those needed to determine gas flow rate, the gages were specified to be accurate to 0.1 percent of full scale. Since 100 psi gages were used, accuracy was within 0.1 psi. Certified calibration indicated accuracy was within the specification.

Pressure drop through the receiver tube was measured only during the initial tests. Measurement was made by visual, direct-reading diaphragm differential gage with a maximum range of 3 inches of water. The accuracy was ±2 percent of full scale or a maximum error of .06 inch of water. For the endurance test, there was no attempt to measure the receiver tube pressure drop. This was due to the placement of the relatively high pressure drop flow mixers within the tubes that would have completely overshadowed the receiver tube measurement.

Rotameters were used to measure helium-xenon flow rate. The instruments were calibrated by a positive displacement wet test meter that was accurate to 1 percent of the flow rate in the range of use. Air was used as the calibrating fluid at the same density as expected for the test condition with helium-xenon. The actual difference in density was duly accounted for.

A mass spectrometer was used to ascertain the composition of the working fluid. The mass spectrometer was connected to both the fluid in the gas loop and to the gas supply. In this way, the gas supply served as a reference with which to compare the gas in the system. Care was taken to change the conditions of the gas entering the instrument as little as possible so that the only variable in output would be gas composition. The accuracy of the mass spectrometer is very much dependent on the scale of measurement, i.e., whether the gas component that is measured is a major constituent or a minute contaminant of the sample. In both cases, error is introduced by electrical "noise"

and drift. For the major constituents, the overall accuracy is within 2 percent of full scale readout, or in terms of its molar percentage the helium reading is accurate to ± 1.3 percent and xenon to ± 2.1 percent. The overall accuracy for the detrimental contaminants, oxygen and nitrogen, is within 1 molar ppm of the reading.

EXPERIMENTAL PROCEDURE

The test on 3 solar receiver tubes was originally conceived in two phases - a short-term test to evaluate performance, and an endurance test to determine any change in performance over a relatively long period of time. A comparison of the two tests is shown in the following tabulation.

	Short-Term Test	Endurance Test
Test Duration	131 hours	2002 hours
Tube Surface	Coated with Fe_2TiO_5	Grit blasted
Basis of Heat Flux	Incident Solar Flux	Incident Solar Flux plus receiver cavity reflectors

In the first test, a coating of Fe_2TiO_5 (iron titanate) was used to increase the emissivity and solar absorptance of the tubes. The iron titanate was in the form of powder which was plasma-sprayed onto the tubes, reflectors, and backing sheet. In the second test, the bare columbium surfaces of 3 new tubes were grit blasted by Al_2O_3 particles, again to increase the emissivity and solar absorptance. The solar flux incident upon the tubes was calculated from the reflection from a 30-foot parabolic mirror and a solar half angle of $0^{o}16'$. The incident flux distribution is shown as the higher peaked curve in figure 12. The curve was obtained through use of a computer code developed by Shrenk (ref. 5). The short-term test was based on full absorption of the incident solar flux. For the endurance test, the net input flow to the tubes was used. This flux distribution, seen as the second curve in figure 12, is also based on the incident solar flux but is reduced by loss through the receiver aperture and the reflective interchange within the receiver cavity. The full analysis resulting in this curve is described in reference 1.

The 3-tube test was designed to operate at the same condition of gas flow per tube as in a solar receiver Brayton system

11 kWe unit. The cycle information is as follows:

Working fluid:	helium-xenon gas mixture
Molecular weight:	83.8
Total flow rate through receiver:	1.6 lb/sec
Gas inlet temperature:	1098° F
Gas exit temperature:	1500° F
Gas pressure:	53 psia

Performance evaluation was based on the physical results of the test - dimensionally, metallographically - and on test data such as temperature on the convoluted tube surface and on the backing sheet, the discharge gas temperature, and pressure drop.

The environmental condition that was to be simulated was that of vacuum and a cyclic heat loading of 60 minutes sun, 36 minutes shade. This condition is equivalent to a near-Earth orbit, the plane of which includes the Sun-Earth line. In an actual orbital mission, however, the duration of shade can vary from 0 to 36 minutes, the extent of variation depends upon the angle of the orbit with the ecliptic plane. A constant shade time of 36 minutes each cycle, therefore, imposes a condition of minimum integrated heat input per orbit to the receiver tubes.

The sun-shade simulation was provided by an integral unit incorporating both the timing sequence function and the power controllers. The timing was controlled by a constant-speed rotating drum. Tabs on the drum were positioned to switch the sun condition power setting or the shade condition power setting into the circuit at the appropriate time. Power to the heater was necessary for the shade condition to prevent heat loss through the heater surface. In the first test, there was one bank of power controllers with which to control the two settings (of sun and of shade). As a result, the power had to be reset manually at every switchover. In the second test, a second bank of controllers was added. With one bank set for the sun condition and the other set for the shade, the operation became entirely automatic.

The precondition for startup included the gas loop pressurized to approximately 70 psia with helium, and the vacuum level within the bell jar in the low 10^{-7} torr range. Startup was initiated by applying power to the primary and guard heaters of the test section. The rate of average temperature rise of the receiver tubes was controlled to stay within the following limits:

At 500^{o} pressure no greater than $5x10^{-5}$ torr.

At 1000^{o} pressure no greater than $1x10^{-6}$ torr.

At 1500^{o} pressure no greater than $5x10^{-7}$ torr.

The limits were based upon information from reference 6. Liquid nitrogen flow through the cold wall within the tank helped maintain the vacuum levels.

Steady-state data were obtained at no-flow, average tube temperatures at 1100^{o}, 1350^{o}, 1525^{o}, and 1600^{o} F. The helium gas was then withdrawn from the loop and replaced with the helium-xenon mixture. The diaphragm compressor was started and valves were adjusted to equalize the flow among the three tubes at design flow rate. The preheaters and getter heaters were adjusted to produce the inlet design temperature of 1098^{o} F. The primary and guard heaters were readjusted to produce average tube temperatures of 1100^{o}, 1300^{o}, 1525^{o}, 1600^{o} F. Steady-state data were obtained, therefore, at 4 tube temperature levels with and without flow. Curves drawn through the data points served to calibrate the test results that followed.

RESULTS AND DISCUSSION

Short-Term Test

Within a short period of time after starting, a trend toward higher tube temperature at the end of each succeeding cycle was noticed. When the maximum temperature reached 1750^{o} F, the flux was reduced by 10 percent and was maintained at this value for the remainder of the test. The pressure drop between the inlet and the discharge was measured to be one inch of water. The reading did not change with the sun and shade periods during a cycle.

The test continued for 131 hours and 82 cycles before concluding in a scheduled shutdown. The test section was cut out of the gas loop, opened up, and photographed. The tubes were then separated from the test section and sectioned to ascertain LiF distribution. The iron titanate coating was metallographically analyzed.

When the test section was opened, figure 13, the tubes appeared to be in good condition physically; there were no apparent distortions of any convolution and no bowing of the tubes. There were, however, whitish zones on the convolutions resembling water stains, figure 14. Consequently, four samples

of the coating were taken for an x-ray diffraction analysis. The samples were taken from the whitish zones of the 1st, 20th, and 30th convolutions of the center tube and from an apparently unaffected zone of a convolution of a flanking tube. The results showed that the iron titanate, Fe_2TiO_5, had decomposed and that the samples from the whitish zones showed the greatest effect. In these areas, there were strong indications of α Fe (free iron) and TiO_2 . The sample from the flanking tube showed strong $FeTiO_3$ and TiO_2 with a medium indication of Fe_2TiO_5. These findings correspond with those of Harrison and Hendrixson, ref. 7, which also showed the whitish zones. Their analyses included picturing the iron in the coating, after test, in large discrete nodules in contrast to the uniform distribution of iron and titanium before test. The breakdown included a releasing of the oxygen to be absorbed by the columbium alloy substrate. Contamination levels of Harrison and Hendrixon reached into the 2000 ppm range after 3000 hours of testing.

The center tube was sectioned lengthwise to ascertain the LiF distribution in each convolution as well as along the length of the tube. Figures 15a, b, and 16a, b, show the views inside the convolutions on the heater (180^o) side and on the opposite (0^o) side respectively. The LiF is shown to have frozen mostly on the heater side which is also that side favored by gravity. The top 5 convolutions are shown to be virtually empty of any salt. Since the salt was loaded at 1750^o F, some of the void volume is attributable to the contraction of the liquid from 1750^o F to its freezing temperature of 1560^o F. This was calculated to be equivalent to approximately 2½ convolutions in the discharge region. The other influence is the effect of gravity in draining off that volume of liquid and distributing it to the convolutions below. The very bottom (inlet region) convolutions appear to include more frozen LiF than some others of equal capacity in the same region. The short-term test indicated areas where improvements were needed to obtain accurate data. These included a closer coupling of the gas temperature sensors to the convoluted tubes and an automated system to switch from a solar power setting to a shade power setting. These features were incorporated for the endurance test.

Endurance Test Results

The endurance test imposed essentially the same conditions on the second set of tubes (consisting of grit-blasted bare columbium-1% zirconium tubes), as on the first set. The imposed heat flux again had to be reduced when the maximum convolution temperature approached 1750^o F. The reduction was 5% of the corrected incident heat flux. The endurance test consisted of 1251 sun-shade cycles and 2002 hours. Shutdown occurred as scheduled.

Upon completion of the endurance test, the test section was cut out of the gas loop, opened up and photographed. The tubes were radiographed and dimensionally measured. The center tube was subsequently sectioned for metallographic analysis. Results of the above steps plus the data from the test are described below.

Physical Features. - The overall impression of the tubes when the test section was opened, figure 17, was that its basic physical integrity was preserved. There were no gross distortions of any convolution nor was there an obvious bowing of the tube axis with respect to each other. The surfaces appeared to be free of cracks and no salt buildup was apparent to suggest LiF leak. There was, however, a blackish deposit on the tubes and on the backing sheet. The deposit (soot-like particles) was heavier toward the inlet end of the tube and virtually nonexistent toward the discharge end. The particles were easily scraped off the tube surface with parchment paper and were subsequently analyzed. The analysis will be described in more detail under "Metallographic Analysis".

The three tubes were radiographed to determine LiF distribution in the convolutions. Figures 18, 19 and 20 show the three tubes at the inlet region, midregion, and exit region respectively. The tubes are in the same relative position to each other except that each tube has been rotated 90^{o}. The view shown, therefore, is essentially that of the tube cross section from the heater (180^{o}) side to the backing sheet (0^{o}) side.

In general, the intent of the convolution design, as evidenced by these radiographs appears to have been successful in distributing LiF along the length of the gas-flowing tube. It is evident, however, that there had been some shift in LiF distribution. The inlet region convolutions appeared to be relatively fuller than the midsection convolutions; and the discharge end region had virtually no LiF in its last several convolutions. Figure 21 shows the first (inlet) convolution of tube No. 2 with its top half cut away revealing the solidified LiF. The fullness of the salt within the convolution corroborates the indication of the radiographs. In addition, the first few convolutions in the inlet region, as seen more clearly in figure 22, appear to be distorted. The heater side of the convolutions appears to have "swelled".

The radiographs in the middle section of the convoluted tubes, figure 19, indicate what had been expected for the entire convoluted tube length. The amount of LiF in each of the convolutions appears to be the same as before the test. The location of the LiF indicates the influence of gravity on distribution within the convolution.

Figure 23 offers the contrast of the LiF taken from convolution #4 near the tube inlet compared to the LiF taken from convolution #18, in the midlength region of the tube. The LiF from convolution #4 appears to be an accumulation of discrete lumps that has taken a number of sun-shade periods to build up. The LiF from convolution #18, on the other hand, is a clear crystalline structure that suggests total LiF melting and freezing during each orbital period.

The radiographs of the convoluted tubes at the exit section all show virtually no LiF in the last 7 or so convolutions. If, as described in the short-term test discussion, the volume of 2½ convolutions can be attributed to the differential contraction between the fill temperature of 1750° F and the freeze temperature of 1560° F, the volume equivalent of 4½ convolutions must have flowed to the convolutions below. This does not mean, however, these 4½ convolutions necessarily remain empty during an entire orbital period. It is possible during the heating period that liquid LiF expands partially into these convolutions from the convolutions below. It does mean that even if this occurs, the LiF drains into the lower convolutions by the end of the shade period.

The changes in dimension after the test are tabulated in table II. The change is defined as the measurement after test minus the measurement before test. The positive sign, therefore, indicates a dimensional increase as a result of the test. Dimension "D" was measured at the 90° and 270° planes before test and at 0°, 90°, 180°, and 270° planes after test. The change in dimension *D at the 0° and 180° planes was defined as the measurement after test minus the average of the measurements at 90° and 270° before test.

Examining table II, the convolution distortion in the inlet region, described qualitatively previously, can be seen in terms of dimensional changes in the ΔD and *D planes. The center tube shows the distortion covering more of the convolutions than the outer tubes. This result can be expected as the two flanking tubes are fulfilling their function as a thermal barrier for the center tube and are expected to be operating cooler than the center tube. The greatest change is in the 180° plane (toward the heater) and extends from the 1st to the 17th convolution.

The distortion of the D dimension had the effect of drawing in the major diameter of the convolution. This can be seen by the negative signs of ΔA in those instances where ΔD and *D were notably high.

The method of measurement involved in tables I and II indicates that caution is in order when determining the significance of some of the values. No inscriptions of any kind were allowed

on the tube material for measurement purposes. The intent of this prohibition was to avoid inducing a crack or other deleterious effects in the convolutions. As a result, there are rough spots that would influence diameter readings. In addition, the "D" dimension - the distance across the flats of a convolution - becomes almost meaningless when the contour becomes a continuously angle-changing curve. Therefore, the ΔD readings in the last few convolutions have been omitted.

Another measurement made was that of camber - the displacement of the tube axis from its true centerline at various stations along the tube length. This measurement was made with V-blocks providing end supports for the tube and with a dial indicator. With the indicator held fixed and its measuring spindle spring-loaded against a convolution, the tube would be rotated through 360°. The minimum and maximum readings would be noted and the planar angles where they occurred. The maximum displacement among the 3 tubes was in tube #2. Again, this is very likely due to the higher heat input to the center tube. The maximum displacement measured 0.294 inch at the 18th and 19th convolutions. The plane of maximum displacement appeared to be slightly off 180° - more like 190°. Within the test section, the tube would have sagged toward the heater.

Convolution Temperature. - Thermocouples were attached to the convoluted tubes at 5 locations along the length of the tube as shown in figure 4. At each location on the center tube, 4 thermocouples were attached to the outer diameter, or peak, of one convolution - at the 0°, 90°, 180°, and 270° planes. In addition, a thermocouple was attached at the (upper) neck of the convolution on the 180° plane. On the flanking tubes, thermocouples were attached at the convolution peak on the 180° plane at each location. These thermocouples were intended to confirm the readings on the center tube. The convolutions that were instrumented were Nos. 3, 9, 19, 28 and 35.

Figures 24 through 28 present the variation of temperature at each location on the center tube during the 1240th cycle (near the end of the endurance test period). The pattern in the 3rd convolution, figure 24, indicates that the temperature at the 180° peak position was in the molten LiF temperature range for most of the sun period and was distinctly higher than the temperature in the other positions. The temperature in the 90° peak position, in contrast, remained entirely in the solid LiF temperature range. The thermocouple at the 0° peak position became inoperative early in testing but undoubtedly would have been indicating the coldest temperatures. A significant reading is the temperature at the 180° neck position. The temperature is seen to increase to above 1560° F and presumably to have melted the LiF. A passage of molten LiF would have allowed accessible

liquid LiF in the convolution above to have flowed into the voids of convolution 3. The reason for the subsequent temperature drop while still in the sun period is not entirely understood. The reading was considered valid, however, since the 28th convolution also showed the same occurrence. This phenomenon is most obviously seen in figure 27 at the 180° neck and the 90° peak positions. Though the exact sequence of events might not be determinable, the cause of the phenomenon is easily recognized. The LiF within the convolutions was designed to function in the two-phase region; therefore, the operational condition was that of continuing change. Not only was there a constant melting and freezing of LiF, but also a change-of-phase volumetric expansion and contraction. Both of these factors contribute to a constant shifting of liquid, solid, and void solumes within each convolution. The many inflections that are common to many of the temperature curves further testify to the complex processes that took place.

Figure 25 presents the temperature variation of the 9th convolution. The general temperature distribution - the large difference between the temperature at the 180° peak position and the other clustered temperatures - is similar to the distribution at the 3rd convolution. The temperature variation at the 180° peak position, however, appears to have undergone a transition. Instead of a more or less constant rate of temperature rise during the sun period, the temperature began at a lower level and suddenly rose about 40° over the last 20 minutes. This behavior is characteristic of a single phase response to heat input. In other words, the curve suggests that the controlling condition within the convolution, at the 180° peak position after 40 minutes, was that due to liquid LiF. The change in conditions can only be attributed to the continuously changing relationship of the solid and liquid phases of the salt and the void volume.

The temperature distribution and variation on the 19th and 28th convolutions are similar, as seen in figures 26 and 27. All of the temperatures appear to be responding in concert and within a range of 25° of one another. All the curves show a relatively sharp increase during the sun period similar to the curve discussed for the 9th convolution. The reason for the sharp rise would be the same also - the LiF having melted entirely and further heat input resulting in the temperature rise of the LiF. As mentioned previously, there were instances of the temperature actually decreasing during the sun period such as shown in figure 27. It should be mentioned also that there were instances of a temperature increase during the shade period. All of the figures of the 19th and 28th convolutions include at least one curve showing this phenomenon.

Again, the reason for the apparent deviation is due to the mixture of the 2 phases of the salt and the void volume.

Figure 28 reflects the result of one of the exit region convolutions devoid of LiF. In this convolution (No. 35), the temperature spread is widened to as much as 70^{o} - in contrast to the 25^{o} spread of the previous two locations. Because of the shallow convolutions as well as the total void, there is little temperature difference between the peak and the neck at the 180^{o} position. It may be noted that in this region where the latent heat consideration is absent and with a constant power input to the heaters, that the temperatures after the first 15 minutes in the sun period, increase at a low rate. It is evident that there is an equilibrium condition reached whereby a tendency for an increase in temperature is offset by reradiation. The equilibrium temperature under the given conditions was 1665^{o} F. Other locations too exhibit the temperature tapering off after an initial sharp rise. This would indicate that even with the presence of LiF, the temperature of the convolution would increase after LiF melting until an equilibrium condition is reached. For the 19th and 28th convolutions, the maximum equilibrium temperature was 1633^{o} F.

Helium-Xenon Performance. - The working gas, helium-xenon, was maintained at a constant flow rate and inlet temperature. The discharge temperature was recorded daily throughout the endurance test. Figure 29 shows the discharge gas temperature during a full cycle at the beginning, middle, and towards the end of the test. The curves appear to exhibit the same trends as the convolution temperatures. The temperature increases relatively rapidly at the beginning of the sun period and then tends to level off. At the end of the sun period, the gas temperature drops sharply and again tends to level out. The curves themselves are not smooth but rather made up of a series of small steps and plateaus. This suggests that the curve reflects the result of each convolution's contribution to the total heat input to the gas.

All three curves are shown having operated on both sides of the design value of 1500^{o} F. The gas temperatures ranged from 29^{o} below to 50^{o} above the design temperature. Comparison of the curves indicates that the gas was receiving more heat as the test progressed. The difference between the minimum and maximum temperatures was 65^{o}, 72^{o} and 75^{o} for the 32nd, 728th, and 1251st cycles respectively. For the 32nd and 728th cycles, the discharge temperature was above 1500^{o} F for 56 minutes. For the 1251st cycle, the time was 65 minutes.

Metallographic Analysis. - Metallographic analysis was performed upon (1) the blackish deposit on the tubes and the V-gutter

heat shields and (2) the refractory material of the convolutions, V-gutter heat shields, and the heater wire. Attention was directed upon the center tube for the analyses.

The blackish deposit was obtained from the tubes and, separately, from the V-gutters. The deposit was analyzed spectrographically, by x-ray diffraction, and by an electron microprobe. The deposits in both cases indicate that the major constituents are columbium and aluminum. The spectrographic analysis also indicated a moderate amount of iron and titanium. This finding would indicate that iron titanate was still present despite the attempt to eliminate the coating from within the test section. The presence of aluminum raises the question as to its source. There are three possibilities - all pertaining to aluminum oxide (Al_2O_3). The first is its use as a powder that grit-blasted the surfaces exposed to the heat flux. There is a possibility that tiny particles may have become embedded in the grit-blasted surface. A second possible source is its use as insulating sleeves for the thermocouples used throughout the test section. The third possibility is its use as electrical insulators separating the tantalum heater wires from its support frame. The purity of the aluminum oxide used in the first two cases was 99.5% or better. A photograph of the deposit, shown in figure 30, suggests a coral-reef type of structure. Figure 31 contrasts the deposit with the bare columbium metal. Investigation is continuing to trace the source of the aluminum.

Analyses were also conducted on the convolution material, V-gutter heat shield, and a section of the tantalum heater wire. Material from the 4th, 18th, and the 35th convolutions (inlet, middle, discharge regions respectively) were used as specimens. Samples of the V-gutter and heater wire were taken in the high heat flux regions - approximately in the 4th convolution region. Analyses were conducted for oxygen, nitrogen, and carbon contents. The tests were performed by the inert gas fusion, Kjeldahl, and combustion chromatographic methods, respectively. All three convolutions indicated no difference in nitrogen content (71-82 ppm) or in carbon content (22-59 ppm). There was a definite gradation of oxygen content, however. The 4th convolution showed the highest reading, 2200 ppm; the 18th showed a lower value, 1200 ppm, and the 35th showed the least, 500 ppm. The original columbium-1% zirconium had less than 100 ppm oxygen, 50 ppm and less of nitrogen, and less than 50 ppm of carbon. The V-gutter heat shield sample had a reading of oxygen content that was in the same range as that of the 4th convolution. The tantalum heater wire, however, had an oxygen reading of 125 ppm, a nitrogen reading of 8 ppm, and carbon of 30 ppm. Investigation is continuing.

Endurance Test - Discussion of Results

The results from the endurance test can be classified into two categories. The first concerns those parameters for which the test was instrumented - such as the temperature and pressure readings. These results have been covered adequately in the previous discussion. The second category consists of those results which were largely unpredictable from an analytical standpoint and which depended upon the test for qualitative insights and quantitative data. These phenomena include the nature of the distortions of the convolutions and the shift in distribution of the LiF along the tube length. The following discussion deals with this second category of results.

A cursory inspection of the convolutions of the tubes and the radiographs initially suggested a correlation between salt fullness and distortion. Certainly the inlet region showed very marked evidences of both. Further investigation, however, which included dimensional measurements of the convolutions and a careful removal of the convolution shell to inspect the frozen LiF within, suggests that the two phenomena - that of salt fullness and extent of distortion - were primarily due to separate mechanisms.

Convolution distortion appears to have taken place because of the insufficient local void volume available when passing from the shade to the sun periods. An essential ingredient bringing about this condition within an individual convolution is that of gravity. The single convolution tilted as it is when the tube axis is oriented $22\frac{1}{2}^{o}$ from the vertical, enables gravity to exert force on the salt to flow toward the "low" side which happens in this test to be the side of the heat source. The consequence is that during the shade period, as the salt starts freezing (and shrinking), the liquid tends to fill any developing void volume on the heater ("low") side of the convolution. The resulting distribution, as seen in the radiographs, shows a concentration of the salt on the heater side of the convolution and much of the void on the "cold" side. When the shade period passes to the sun, melting takes place on the heater side where the void volume is limited. When the void volume is filled, further melting causes the convolution wall in that local sector to distort to accommodate the liquid salt.

The convolution temperatures in figures 24 and 25 tend to confirm the above description. These two figures plot the surface temperatures on the two instrumented convolutions (#3 and #9) that were distorted. The temperature at the top (nearest the heater) peak location is seen to pass through the melt temperature before that of any other location. Not

only does this sector of the convolution reach melt temperature first, but its temperature is well into the melt region while other sectors within the same convolution remain within the frozen temperature region for much, if not all, of the total cycle. The apparent aberrations in some of the temperature curves may well be explained by the flow processes within the individual convolution as described previously.

Salt fullness, on the other hand, is brought about by the condition of incomplete melting of the salt within a convolution in addition to gravity. Incomplete melting in the first few convolutions was anticipated. Figure 32, which is reproduced from reference 1, shows the discrepancy between the heat input shown as broken lines and the potential for cooling if the convolution temperature was at 1560° F shown as a solid line. Clearly the first few convolutions were overcooled. At the end of the sun period, without the addition of salt external to a convolution, we could expect void volume proportional to the salt not melted. The convolution temperature distribution, figure 24, does indicate however that the neck reaches melt temperature during the sun cycle. This would enable the molten salt from the convolution above to flow down by gravity into the existing void volumes. The additional salt to the convolution from above may be compensated to an extent by the loss of the molten salt to the convolution below. The lowest convolution (#1) eventually approaches a condition of fullness where it cannot accept any additional amounts of salt. Actually a small amount will still enter to the extent that distortion (as described previously) has provided more total volume in the convolution. The next higher convolution thereafter approaches its condition of fullness as does the succeeding convolutions in sequence.

CONCLUDING REMARKS

The purpose of the three-tube tests was to obtain performance data and to gain an understanding of the mechanisms involved in transferring heat under simulated near-Earth orbital conditions. While the sun-shade periods and the vacuum environment could be controlled or ascertained, the condition of zero-gravity obviously could not be attained. Although the design was selected to minimize the effect of operation in gravity, the physical results of the test were heavily influenced by the gravity effect. In an environment of zero- or low-gravity, a maldistribution resulting in a high concentration of LiF in some convolutions and totally void of LiF in others, to the extent encountered in the test, most certainly would not have occurred. Given the condition of Earth gravity, however, the results herein should be regarded as having been obtained under a much more stringent circumstance than zero-gravity.

After 2002 hours of testing, the tubes remained intact - no cracks in the columbium tubes and no leakage of LiF. The distortions were local. Equally important, the maldistribution and distortions had little effect on the thermal and hydraulic performance of the receiver tubes. With the last 7 convolutions devoid of LiF, the tubes still functioned to heat helium-xenon, the working gas, to above the design temperature of 1500° F for most of the 96-minute cycle. The He-Xe discharge temperature varied from 30° below to 50° above design. This represents a range of 6 percent below to 10 percent above the design temperature rise of the gas; or -1.5 to +2.5 percent variation from design absolute temperature.

There was some oxygen contamination of the columbium alloy throughout the length of the tubes but heaviest in the inlet region (2200 ppm in the 4th convolution). The source of the contamination has not been traced as yet - but is suspected to be due to the factors peculiar to the test set-up rather than to any source integral to the tube themselves. It is significant that with this level of contamination, the convolutions could still operate with distortion but without cracking or leaking.

The endurance test originally began with the heat flux to the tubes based on full solar heat input (with reflections and reradiation). That this heat input had to be reduced by 5 percent substantiates the design intent of providing a margin of capability in the receiver. In the actual receiver, controllable doors will allow excess heat rate to radiate into space. This margin of capability is further enhanced if it is realized that the sun-shade periods selected for the test were based on minimum sun and maximum shade values. In an actual orbital mission, there would be generally a higher percentage of the sun period.

For flux input that was 95 percent of the full design value, the maximum convolution temperature was 1670° F. This value is well within the limitation of the material.

If the question remains regarding what further steps can be taken so that LiF remains within each compartment - one answer would be to ensure that the LiF in the neck of each convolution is always solid (frozen). In this way, each convolution would have its original "allotment" of LiF to which nothing would be added or subtracted. If the LiF is properly distributed initially, the only way for overexpansion to occur is in the case of the average convoluted tube temperature reaching 1750° F - the maximum temperature for which it was designed. One step toward accomplishing this end is to insert a columbium alloy collar around the neck of each convolution to form a barrier to the thermal radiation.

REFERENCES

1. Burns, Raymond K.: Preliminary Thermal Performance Analysis of the Solar Brayton Heat Receiver. NASA TN D-6268, 1971.

2. McKinnon, R. A.; and Kamperman, E. F.: Sunflower Boiler/Heat Storage Topical Report. Rep. ER-4869, TRW, Inc., Apr. 1963.

3. McKinnon, R. A.; Vild, T. J.; and Milko, J. A.: Design Study of Solar Absorbers with Lithium Fluoride Heat Storage. Space Power Systems Engineering. G. C. Szego and J. E. Taylor, eds., Academic Press, 1966, pp. 795-820.

4. Anon.: Brayton Cycle Cavity Receiver Design Study. Rep. ER-6497, TRW, Inc. (NASA CR-51752), Nov. 22, 1965.

5. Shrenk, G. L.; and Gritton, D. G.: Analysis of Solar Reflectors. Mathematical Theory and Methodology for Simulation of Real Reflectors. Final Report, Allison Division, General Motors Corp., 1963. (Available from DDC as AD-602870.)

6. Holowach, J., ed.: Advanced Refractory Alloy Corrosion Loop Program. Test Plan for T-111 Rankine System Corrosion Test Loop. Rep. GESP-2[illegible], General Electric Co. (Work under contract NAS3-6474).

7. Hoffman, E. E.; and Holowach, J.: The Cb-1Zr Rankine System Corrosion Test Loop. NASA CR-1509, 1970.

TABLE I(a). - DIMENSIONS OF RECEIVER TUBE NO. 1 BEFORE TEST

Dimension @	A		B		C		D		
Orientation	90°-270°	0°-180°	90°-270°	0°-180°	90°	270°	90°	270°	avg.
Convolution no. 1	3.289	3.284	1.330	1.330	0.97	0.98	0.641	0.644	0.642
2	3.296	3.296	1.327	1.330	1.95	1.94	0.631	0.639	0.635
3	3.299	3.303	1.329	1.333	2.92	2.93	0.633	0.638	0.636
4	3.298	3.297	1.333	1.332	3.91	3.88	0.631	0.637	0.634
5	3.296	3.291	1.334	1.334	4.90	4.85	0.638	0.634	0.636
6	3.300	3.305	1.336	1.335	5.88	5.87	0.645	0.637	0.641
7	3.274	3.272	1.333	1.332	6.84	6.80	0.615	0.622	0.618
8	3.213	3.219	1.331	1.333	7.78	7.77	0.580	0.585	0.582
9	3.186	3.182	1.335	1.330	8.75	8.74	0.609	0.612	0.610
10	3.141	3.139	1.332	1.335	9.74	9.73	0.626	0.625	0.626
11	3.095	3.100	1.331	1.332	10.71	10.69	0.586	0.589	0.588
12	3.064	3.064	1.328	1.330	11.64	11.64	0.586	0.587	0.586
13	3.010	3.014	1.325	1.330	12.62	12.61	0.550	0.548	0.549
14	2.977	2.975	1.331	1.329	13.56	13.57	0.578	0.586	0.582
15	2.935	2.938	1.325	1.329	14.53	14.55	0.587	0.594	0.590
16	2.891	2.888	1.322	1.324	15.49	15.52	0.565	0.566	0.566
17	2.849	2.842	1.327	1.324	16.45	16.49	0.556	0.554	0.555
18	2.822	2.817	1.331	1.330	17.42	17.44	0.588	0.580	0.584
19	2.763	2.767	1.328	1.330	18.36	18.40	0.569	0.567	0.568
20	2.733	2.734	1.332	1.328	19.33	19.38	0.578	0.573	0.576
21	2.694	2.696	1.331	1.332	20.31	20.36	0.588	0.584	0.586
22	2.640	2.645	1.327	1.330	21.26	21.30	0.556	0.548	0.552
23	2.602	2.600	1.329	1.324	22.23	22.26	0.549	0.542	0.546
24	2.569	2.571	1.325	1.328	23.19	23.23	0.555	0.553	0.554
25	2.531	2.530	1.326	1.331	24.14	24.18	0.572	0.558	0.565
26	2.488	2.489	1.331	1.327	25.11	25.16	0.554	0.550	0.552
27	2.455	2.446	1.329	1.332	26.08	26.12	0.545	0.542	0.544
28	2.413	2.413	1.324	1.323	27.08	27.07	0.565	0.548	0.556
29	2.377	2.379	1.324	1.328	28.06	28.05	0.555	0.547	0.551
30	2.331	2.329	1.328	1.326	29.04	29.03	0.556	0.562	0.559
31	2.298	2.300	1.327	1.328	30.02	30.02	0.579	0.590	0.584
32	2.247	2.248	1.322	1.329	31.00	31.00	0.582	0.569	0.576
33	2.220	2.219	1.321	1.326	31.98	31.98	0.591	0.588	0.590
34	2.184	2.187	1.326	1.322	32.96	32.96	0.600	0.587	0.594
35	2.143	2.137	1.330	1.328	33.94	33.96	0.616	0.615	0.616
36	2.087	2.085	1.332	1.328	34.95	34.95	0.585	0.592	0.588
37	2.055	2.062	--	--	--	--	0.598	0.563	0.576

@ Dimensions are shown in Figure 7. All measurements are in inches.

TABLE I(b). - DIMENSIONS OF RECEIVER TUBE NO. 2 BEFORE TEST

Dimension @	A		B		C		D		
Orientation	90°-270°	0°-180°	90°-270°	0°-180°	90°	270°	90°	270°	avg.
Convolution no. 1	3.278	3.280	1.329	1.329	1.01	0.97	0.654	0.634	0.644
2	3.301	3.298	1.328	1.328	1.98	1.95	0.631	0.630	0.630
3	3.294	3.288	1.328	1.329	2.97	2.92	0.625	0.629	0.627
4	3.297	3.298	1.320	1.324	3.93	3.90	0.629	0.627	0.628
5	3.299	3.300	1.329	1.328	4.91	4.88	0.621	0.619	0.620
6	3.292	3.296	1.329	1.326	5.87	5.87	0.624	0.633	0.628
7	3.263	3.261	1.330	1.331	6.83	6.83	0.596	0.601	0.598
8	3.212	3.215	1.330	1.327	7.81	7.78	0.588	0.579	0.584
9	3.182	3.174	1.329	1.324	8.81	8.77	0.614	0.616	0.615
10	3.136	3.132	1.332	1.329	9.80	9.76	0.618	0.627	0.622
11	3.095	3.101	1.321	1.328	10.78	10.75	0.622	0.622	0.622
12	3.051	3.052	1.328	1.325	11.75	11.69	0.584	0.583	0.584
13	3.007	3.006	1.327	1.331	12.71	12.67	0.553	0.554	0.554
14	2.978	2.976	1.330	1.331	13.69	13.64	0.599	0.603	0.601
15	2.933	2.932	1.330	1.329	14.67	14.61	0.611	0.604	0.608
16	2.896	2.895	1.321	1.324	15.61	15.58	0.571	0.576	0.574
17	2.854	2.852	1.333	1.334	16.56	16.55	0.558	0.564	0.561
18	2.826	2.821	1.332	1.329	17.53	17.52	0.591	0.594	0.592
19	2.771	2.764	1.332	1.333	18.53	18.48	0.574	0.579	0.576
20	2.731	2.733	1.337	1.334	19.52	19.45	0.587	0.580	0.584
21	2.695	2.696	1.338	1.335	20.50	20.44	0.599	0.610	0.604
22	2.650	2.651	1.331	1.331	21.48	21.42	0.574	0.590	0.582
23	2.608	2.611	1.330	1.329	22.46	22.37	0.557	0.564	0.560
24	2.571	2.570	1.326	1.323	23.42	23.34	0.570	0.581	0.576
25	2.536	2.532	1.333	1.333	24.38	24.32	0.586	0.577	0.582
26	2.487	2.492	1.333	1.337	25.36	25.31	0.562	0.570	0.566
27	2.446	2.450	1.335	1.335	26.35	26.28	0.566	0.564	0.565
28	2.410	2.412	1.324	1.321	27.33	27.25	0.564	0.568	0.566
29	2.373	2.372	1.331	1.325	28.29	28.22	0.563	0.560	0.562
30	2.326	2.324	1.327	1.326	29.27	29.22	0.583	0.580	0.582
31	2.290	2.286	1.321	1.320	30.24	30.19	0.564	0.574	0.569
32	2.243	2.245	1.323	1.323	31.22	31.18	0.590	0.593	0.592
33	2.213	2.213	1.327	1.324	32.21	32.16	0.600	0.601	0.600
34	2.184	2.187	1.327	1.325	33.17	33.12	0.588	0.598	0.593
35	2.145	2.146	1.320	1.324	34.15	34.12	0.620	0.634	0.627
36	2.085	2.087	1.330	1.324	35.16	35.14	0.596	0.614	0.605
37	2.056	2.066	--	--	--	--	0.576	0.585	0.580

@ Dimensions are shown in Figure 7. All measurements are in inches.

TABLE I(c). - DIMENSIONS OF RECEIVER TUBE NO. 3 BEFORE TEST

Dimension @	A		B		C		D		
Orientation	90°-270°	0°-180°	90°-270°	0°-180°	90°	270°	90°	270°	avg.
Convolution no. 1	3.281	3.276	1.330	1.332	0.98	0.95	0.640	0.638	0.639
2	3.307	3.302	1.330	1.327	1.93	1.91	0.629	0.636	0.632
3	3.305	3.302	1.334	1.332	2.89	2.87	0.627	0.638	0.632
4	3.302	3.299	1.329	1.331	3.87	3.87	0.631	0.650	0.640
5	3.308	3.305	1.331	1.332	4.84	4.80	0.628	0.637	0.632
6	3.304	3.305	1.333	1.333	5.79	5.79	0.626	0.631	0.626
7	3.271	3.274	1.330	1.327	6.75	6.69	0.612	0.619	0.616
8	3.224	3.220	1.327	1.333	7.67	7.67	0.574	0.586	0.580
9	3.189	3.190	1.328	1.329	8.63	8.61	0.602	0.610	0.606
10	3.131	3.133	1.333	1.333	9.61	9.57	0.611	0.616	0.614
11	3.098	3.097	1.332	1.332	10.57	10.54	0.593	0.586	0.590
12	3.055	3.056	1.324	1.325	11.53	11.50	0.580	0.579	0.580
13	3.011	3.002	1.325	1.327	12.49	12.47	0.543	0.545	0.544
14	2.978	2.979	1.328	1.328	13.46	13.43	0.604	0.596	0.600
15	2.935	2.940	1.323	1.327	14.42	14.41	0.603	0.595	0.599
16	2.898	2.900	1.327	1.323	15.38	15.39	0.571	0.573	0.572
17	2.853	2.854	1.328	1.327	16.33	16.35	0.570	0.569	0.570
18	2.821	2.822	1.330	1.330	17.31	17.31	0.595	0.594	0.594
19	2.756	2.754	1.330	1.328	18.27	18.29	0.578	0.568	0.573
20	2.740	2.738	1.330	1.333	19.25	19.28	0.581	0.576	0.578
21	2.695	2.698	1.330	1.331	20.21	20.23	0.590	0.593	0.592
22	2.647	2.644	1.324	1.328	21.19	21.21	0.566	0.562	0.564
23	2.614	2.615	1.327	1.327	22.14	22.18	0.558	0.550	0.554
24	2.567	2.575	1.323	1.324	23.12	23.14	0.566	0.562	0.564
25	2.541	2.539	1.329	1.327	24.09	24.12	0.569	0.568	0.568
26	2.493	2.493	1.327	1.328	25.06	25.08	0.552	0.552	0.552
27	2.448	2.456	1.330	1.326	26.04	26.04	0.562	0.544	0.548
28	2.415	2.411	1.322	1.328	27.02	27.02	0.554	0.565	0.560
29	2.374	2.373	1.324	1.326	27.98	28.01	0.554	0.550	0.552
30	2.333	2.328	1.329	1.328	28.94	29.00	0.552	0.555	0.554
31	2.295	2.294	1.326	1.320	29.92	29.98	0.576	0.560	0.568
32	2.250	2.252	1.324	1.327	30.93	30.96	0.590	0.570	0.580
33	2.217	2.219	1.324	1.328	31.91	31.94	0.595	0.618	0.606
34	2.183	2.175	1.326	1.327	32.89	32.89	0.596	0.614	0.605
35	2.144	2.147	1.326	1.333	33.89	33.87	0.619	0.609	0.614
36	2.087	2.188	1.329	1.328	34.90	34.88	0.596	0.583	0.590
37	2.056	2.062	--	--	--	--	0.565	0.565	0.565

@ Dimensions are shown in Figure 7. All measurements are in inches.

E-6511

TABLE II (a). - CHANGES IN DIMENSIONS OF RECEIVER TUBE NO. 1 AFTER TEST

Dimension @	ΔA		ΔB		ΔC		ΔD		*D	
Orientation	90°-270°	0°-180°	90°-270°	0°-180°	90°	270°	90°	270°	0°	180°
Convolution no. 1	-.023	-.011	-.005	-.004	+.01	+.01	+.040	+.134	-.004	+.177
2	-.019	-.016	+.004	.000	+.01	+.01	+.075	+.115	+.047	+.132
3	+.003	.000	+.006	+.002	+.01	-.01	+.005	+.006	+.009	+.012
4	+.008	+.009	+.002	+.006	.00	+.02	+.001	+.004	+.011	+.002
5	+.005	+.006	+.003	+.004	.00	-.01	+.006	+.003	+.004	+.009
6	+.005	+.004	+.001	+.001	-.01	-.01	+.012	+.008	+.018	+.019
7	+.005	+.001	+.002	+.002	-.02	+.02	+.010	-.003	.000	+.005
8	+.007	+.006	+.004	+.003	+.01	-.04	+.001	-.007	-.002	+.001
9	+.003	+.006	+.002	+.005	+.01	.00	+.001	.000	+.005	+.004
10	-.003	+.001	+.003	+.001	-.02	.00	+.004	+.007	-.002	+.006
11	+.005	-.003	+.003	-.002	-.02	-.02	+.003	+.010	+.005	+.002
12	+.004	-.002	+.002	+.001	+.01	+.01	+.010	+.003	+.006	+.003
13	-.001	-.003	+.003	-.002	.00	-.02	+.018	+.028	+.018	+.034
14	-.001	.000	+.001	+.002	+.02	+.01	+.016	+.024	+.017	+.025
15	+.005	-.001	+.004	-.004	-.02	.00	+.005	+.005	+.001	-.004
16	-.004	+.007	+.001	+.004	.00	-.01	+.002	+.003	-.002	-.001
17	+.004	+.010	+.002	+.004	+.01	.00	+.004	+.003	+.005	+.002
18	+.001	+.001	+.003	+.004	.00	+.01	+.001	+.014	+.001	+.010
19	+.002	.000	+.001	+.003	.00	.00	-.007	+.009	-.004	+.002
20	+.002	-.001	+.001	+.003	.00	-.03	-.004	+.004	-.006	.000
21	+.002	-.004	+.002	+.001	-.02	-.04	+.004	+.005	+.001	.000
22	+.002	-.003	+.002	+.003	.00	+.03	+.005	+.010	+.007	+.013
23	+.003	+.004	+.002	+.002	.00	+.02	-.003	+.007	+.007	+.006
24	.000	-.004	+.002	+.002	.00	-.04	-.001	+.016	+.026	+.005
25	+.001	+.002	+.003	+.001	+.01	+.06	-.007	+.020	+.012	+.007
26	+.002	+.002	+.002	.000	.00	-.01	-.002	+.009	+.017	+.002
27	+.002	-.007	+.001	+.001	-.01	.00	+.001	+.021	+.016	+.018
28	+.001	+.005	+.002	+.002	+.01	.00	+.002	+.010	+.008	+.004
29	.000	-.002	+.001	+.001	+.01	+.01	+.009	+.022	+.016	+.014
30	+.002	+.002	+.001	+.002	-.02	-.01	+.012	+.015	+.014	+.006
31	-.001	+.001	+.001	-.002	+.02	+.01	--	--	--	--
32	.000	.000	+.002	+.004	.00	.00	--	--	--	--
33	.000	+.002	+.002	-.002	-.01	-.02	--	--	--	--
34	+.001	-.001	.000	+.003	+.01	+.01	--	--	--	--
35	-.001	+.010	+.003	+.002	+.02	-.02	--	--	--	--
36	.000	+.002	.000	+.002	.00	+.03	--	--	--	--
37	.000	-.003	--	--	--	--	--	--	--	--

@ Basic dimensions are shown in Figure 7. All measurements are in inches.
Δ = Measurement after test - measurement before test.
* = Measurement after test - measurement averaged at 90° and 270° before test.

TABLE II(b). - CHANGES IN DIMENSIONS OF RECEIVER TUBE NO. 2 AFTER TEST

Dimension @	ΔA		ΔB		ΔC		ΔD		*D	
Orientation	90°-270°	0°-180°	90°-270°	0°-180°	90°	270°	90°	270°	0°	180°
Convolution no. 1	-.009	-.018	+.001	-.004	+.01	+.03	+.104	+.079	+.043	+.146
2	+.003	.000	+.001	-.002	.00	+.01	.000	+.005	+.013	+.044
3	-.011	-.009	-.002	-.003	.00	+.03	+.093	+.078	+.038	+.153
4	-.015	-.015	-.001	-.004	-.02	-.05	+.081	+.090	+.083	+.107
5	-.017	-.017	-.003	-.004	.00	+.01	+.094	+.087	+.093	+.103
6	-.012	-.016	-.006	-.002	-.01	.00	+.090	+.073	+.080	+.093
7	-.012	-.016	-.006	-.002	-.01	+.01	+.093	+.080	+.087	+.110
8	-.008	-.012	-.002	-.003	+.02	.00	+.064	+.058	+.055	+.090
9	-.005	-.007	-.006	-.005	-.01	.00	+.058	+.058	+.060	+.111
10	-.004	.000	-.001	-.006	.00	-.02	+.051	+.047	+.011	+.110
11	.000	-.006	-.001	-.007	-.01	-.02	+.046	+.031	-.003	+.110
12	-.007	-.007	-.003	-.003	+.01	+.02	+.040	+.036	-.001	+.092
13	-.015	-.015	+.001	-.005	.00	.00	+.057	+.066	+.065	+.081
14	-.009	-.005	-.001	-.009	.00	.00	+.048	+.054	+.031	+.091
15	.000	-.006	.000	-.006	.00	+.03	+.040	+.041	+.029	+.094
16	.000	-.005	+.002	-.002	.00	.00	+.034	+.026	+.026	+.065
17	-.006	-.004	+.001	-.003	.00	.00	+.020	+.018	+.031	+.063
18	+.004	+.001	-.002	.000	+.02	.00	+.022	+.020	+.015	+.020
19	-.001	+.002	-.002	+.001	-.04	+.01	+.012	-.001	+.008	+.008
20	+.002	+.002	-.003	+.001	-.01	-.02	+.006	+.008	+.012	+.005
21	+.009	+.002	+.002	+.001	+.02	-.01	+.006	+.018	+.003	+.002
22	+.004	+.002	+.001	+.002	-.01	.00	+.012	-.006	-.003	-.005
23	+.002	.000	+.002	+.001	-.01	+.02	+.004	+.001	+.013	-.003
24	+.003	-.001	+.002	+.002	.00	.00	+.010	+.008	+.002	-.004
25	+.006	+.002	+.002	+.002	+.02	.00	-.004	+.007	+.004	-.010
26	+.003	-.002	-.003	+.001	-.02	+.01	+.003	+.003	-.001	+.005
27	+.004	+.005	.000	-.002	+.02	+.01	-.008	-.002	+.004	-.016
28	+.010	+.003	+.002	.000	-.02	+.01	+.002	-.006	-.008	+.003
29	+.001	+.002	-.002	+.003	+.01	+.01	-.008	+.003	-.004	-.005
30	+.003	+.003	+.001	+.001	.00	-.03	-.019	-.011	-.021	-.014
31	+.005	-.004	+.001	+.002	+.01	+.02	--	--	--	--
32	+.003	-.001	+.001	+.002	-.01	-.01	--	--	--	--
33	+.005	+.004	+.001	+.003	-.02	+.04	--	--	--	--
34	.000	-.002	+.003	+.002	+.01	+.01	--	--	--	--
35	+.001	-.002	+.002	.000	-.01	-.01	--	--	--	--
36	+.004	+.001	.000	+.004	-.01	-.02	--	--	--	--
37	+.001	-.001	--	--	--	--	--	--	--	--

@ Basic dimensions are shown in Figure 7. All measurements are in inches.

Δ = Measurement after test - measurement before test.

* = Measurement after test - measurement averaged at 90° and 270° before test.

TABLE II(c). - CHANGES IN DIMENSIONS OF RECEIVER TUBE NO. 3 AFTER TEST

Dimension @	ΔA		ΔB		ΔC		ΔD		*D	
Orientation	90°-270°	0°-180°	90°-270°	0°-180°	90°	270°	90°	270°	0°	180°
Convolution no. 1	-.018	-.011	-.002	+.001	+.02	.00	+.123	+.088	+.027	+.152
2	+.001	+.001	+.001	+.001	.00	.00	+.127	+.004	+.003	+.045
3	+.004	-.001	+.004	-.001	+.01	-.01	+.021	+.011	+.005	+.036
4	+.003	+.005	+.004	+.005	-.04	+.01	+.031	+.016	+.018	+.034
5	+.005	+.004	+.005	+.001	+.02	+.02	+.015	+.001	+.011	+.020
6	+.005	+.006	+.004	+.001	+.01	.00	+.018	+.013	+.019	+.028
7	+.007	+.006	+.004	+.003	.00	.00	+.024	+.021	+.020	+.030
8	+.006	+.006	+.004	+.002	+.02	.00	+.010	+.009	+.008	+.016
9	+.005	+.005	+.004	+.005	-.03	.00	+.001	-.004	-.002	-.004
10	+.008	+.006	+.004	+.003	+.02	.00	+.004	+.006	+.003	+.004
11	+.008	+.005	+.002	+.003	-.02	-.01	+.011	+.004	+.009	+.005
12	+.005	+.004	+.004	+.003	+.03	+.01	+.005	+.004	+.006	+.005
13	+.005	+.004	+.005	+.004	-.01	+.02	+.004	+.003	+.003	+.003
14	+.005	+.004	+.003	+.002	-.01	.00	-.004	+.002	+.001	+.002
15	+.004	+.003	+.005	+.003	-.02	.00	+.003	+.001	-.002	-.002
16	+.003	+.003	+.003	+.001	.00	.00	-.003	-.003	-.004	+.005
17	+.004	+.004	+.001	+.002	.00	.00	-.004	-.001	-.007	+.001
18	+.003	+.001	+.002	+.002	+.01	-.01	+.001	-.003	-.003	-.008
19	+.008	+.004	+.003	+.004	.00	.00	-.005	-.002	+.002	-.012
20	+.002	+.003	+.002	+.001	-.01	-.02	+.001	-.002	-.002	+.003
21	+.006	+.003	+.003	.000	+.01	+.01	-.003	-.001	+.003	-.002
22	+.007	+.005	+.005	+.001	-.01	+.01	-.002	-.009	-.001	-.008
23	+.001	+.001	+.002	+.002	.00	-.02	-.005	-.001	-.005	-.001
24	+.003	+.002	+.002	+.001	+.01	.00	+.001	-.004	-.007	+.005
25	+.001	+.002	+.003	+.001	+.01	+.01	+.006	-.003	-.003	+.011
26	+.004	+.002	+.002	+.002	.00	+.02	-.009	+.008	-.007	+.004
27	+.003	.000	+.002	+.002	-.01	.00	-.020	+.014	+.001	+.006
28	+.003	+.004	+.004	+.002	-.02	-.01	-.007	-.015	-.010	-.015
29	+.004	+.002	+.004	+.003	+.02	.00	-.016	-.004	-.008	-.007
30	.000	+.002	+.001	+.002	+.02	.00	-.019	+.010	-.003	-.009
31	+.003	+.002	+.002	+.002	+.01	.00	--	--	--	--
32	+.003	+.003	+.002	-.001	-.02	+.01	--	--	--	--
33	+.003	+.001	+.003	+.001	-.01	.00	--	--	--	--
34	+.006	+.002	+.003	+.001	.00	.00	--	--	--	--
35	+.003	+.003	+.002	-.001	-.01	+.01	--	--	--	--
36	+.003	+.002	.000	.000	+.01	-.03	--	--	--	--
37	-.003	+.002	--	--	--	--	--	--	--	--

@ Basic dimensions are shown in Figure 7. All measurements are in inches.
Δ = Measurement after test - measurement before test.
* = Measurement after test - measurement averaged at 90 and 270 before test.

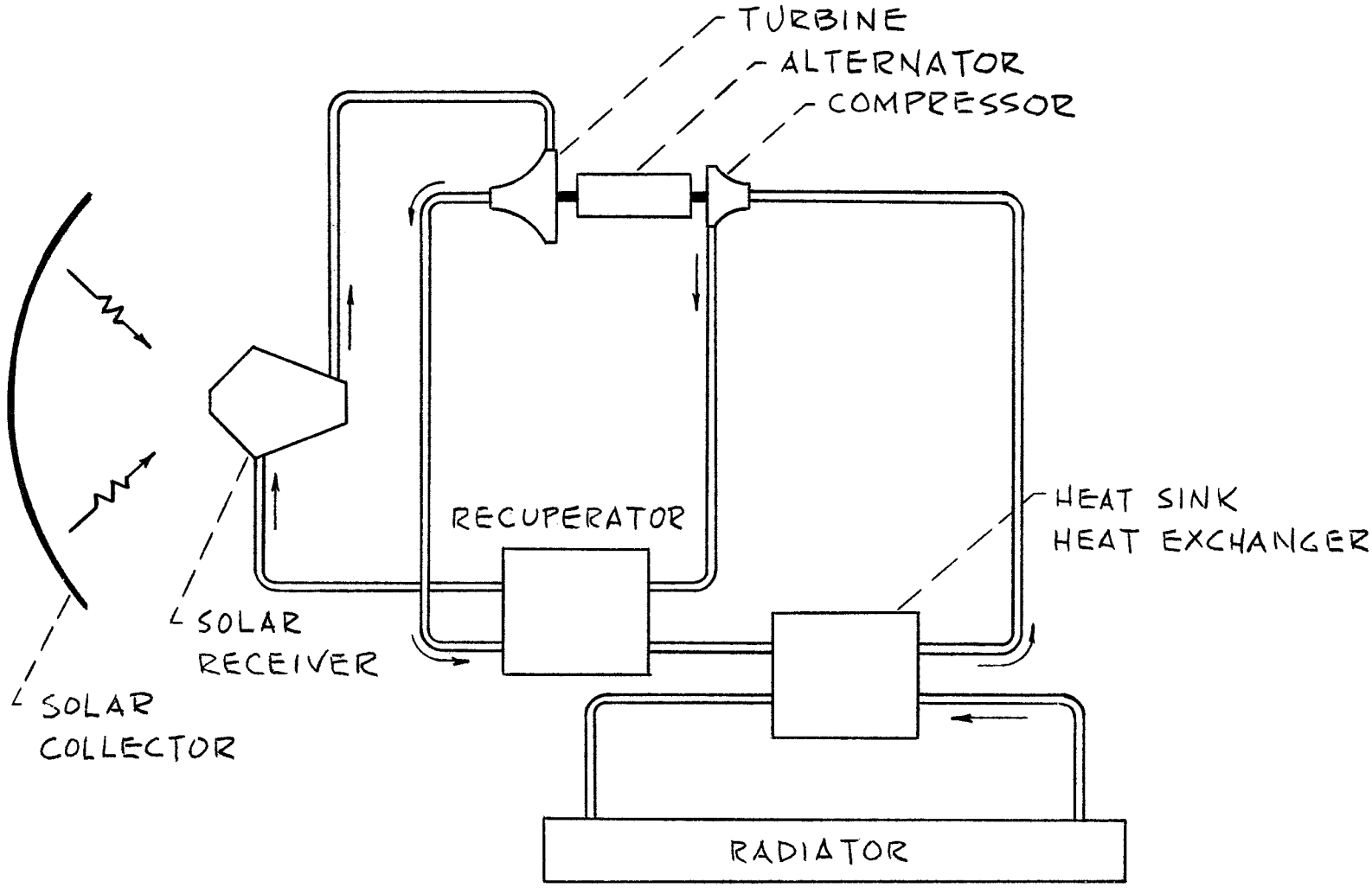

Figure 1: Schematic diagram, Brayton solar-powered system

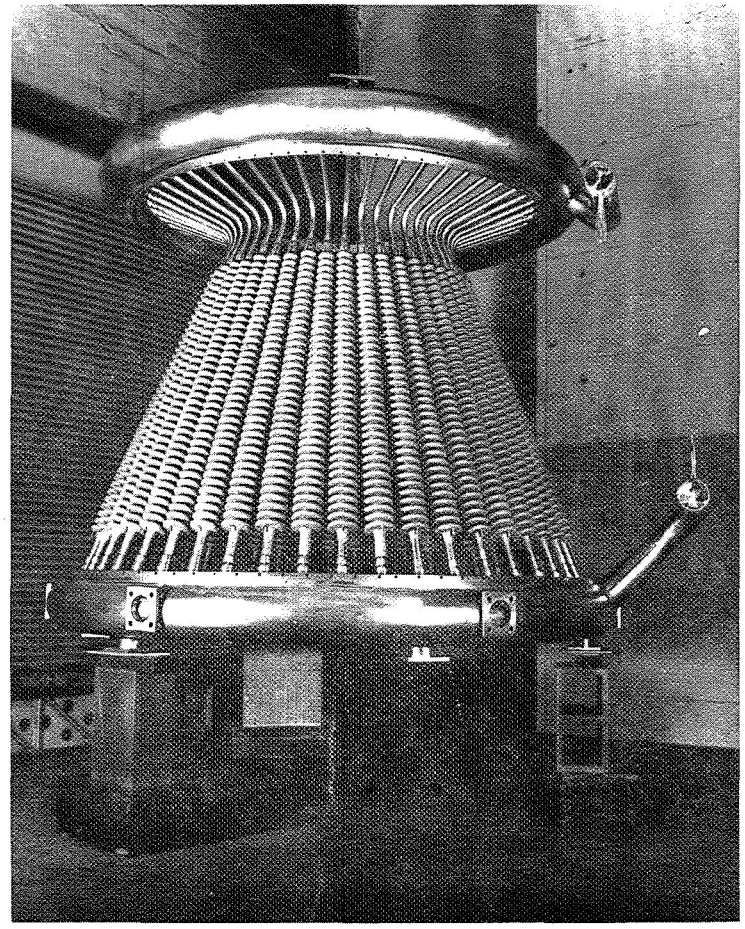

Figure 2. - Brayton cycle solar receiver without heat reflector/insulator shell.

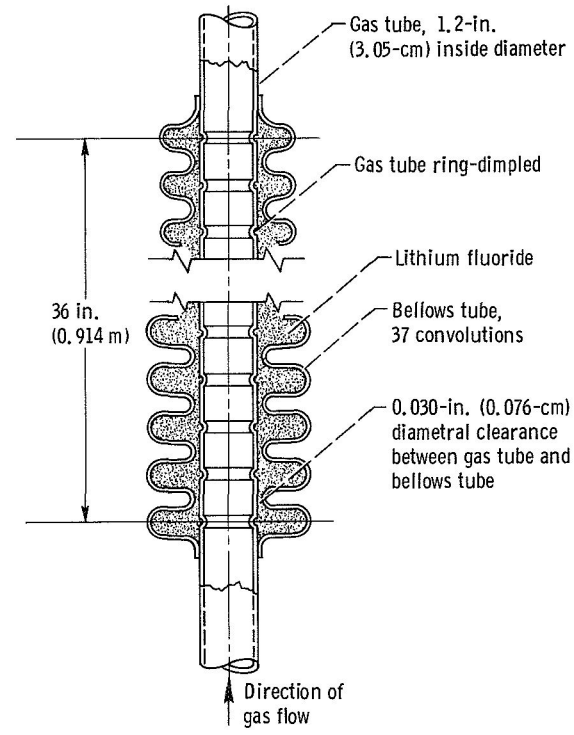

Figure 3. - Heat transfer heat storage tube.

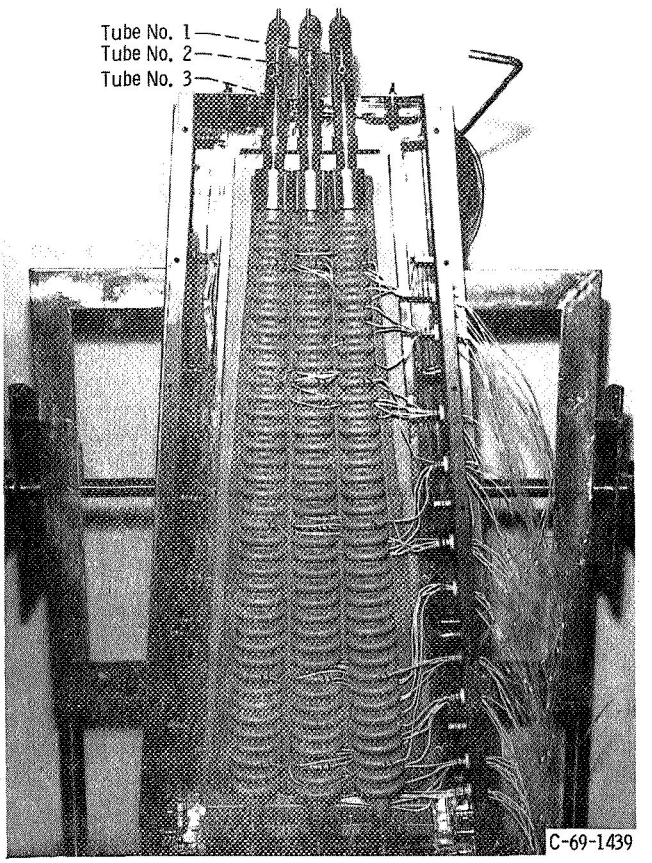

Figure 4. - Test section open showing receiver tubes in position.

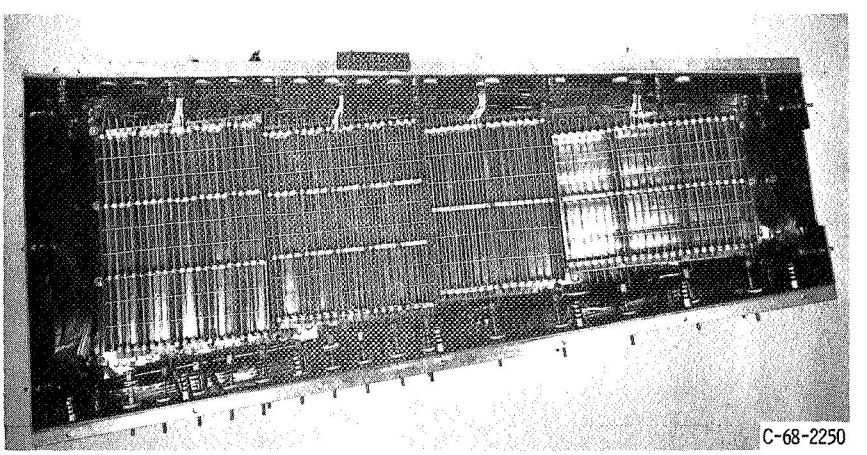

Figure 5. - Test section open showing tantalum heaters.

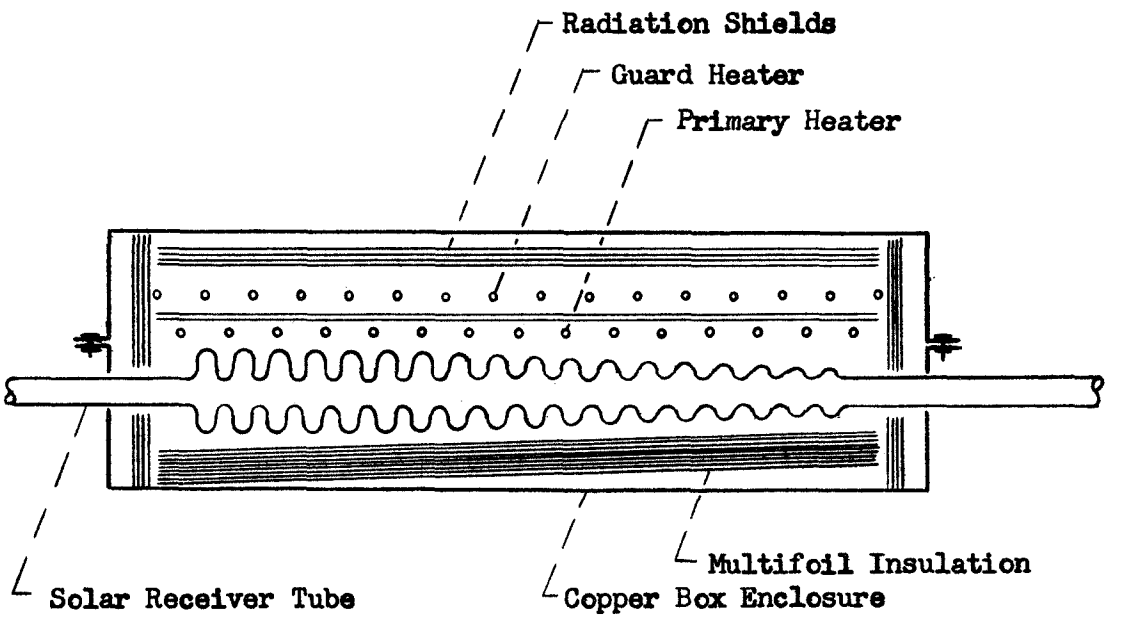

Figure 6: Schematic diagram of cross section through test section showing the relative positions of contents.

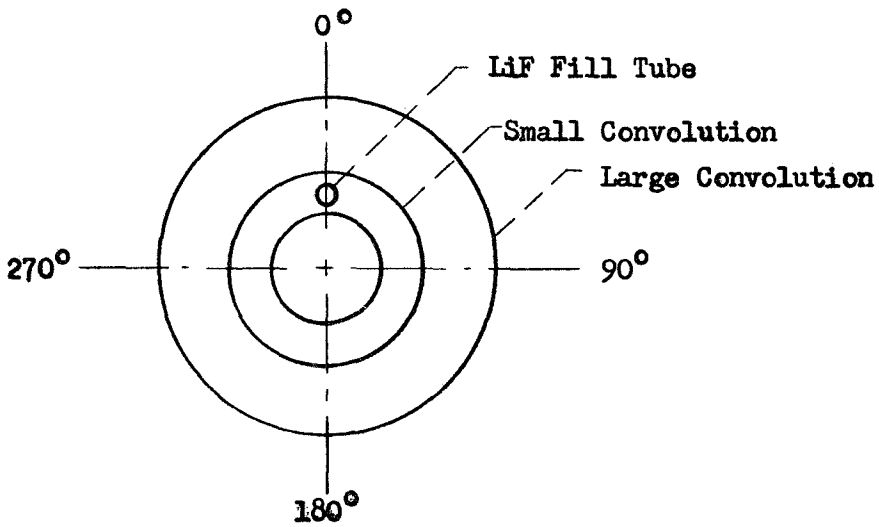

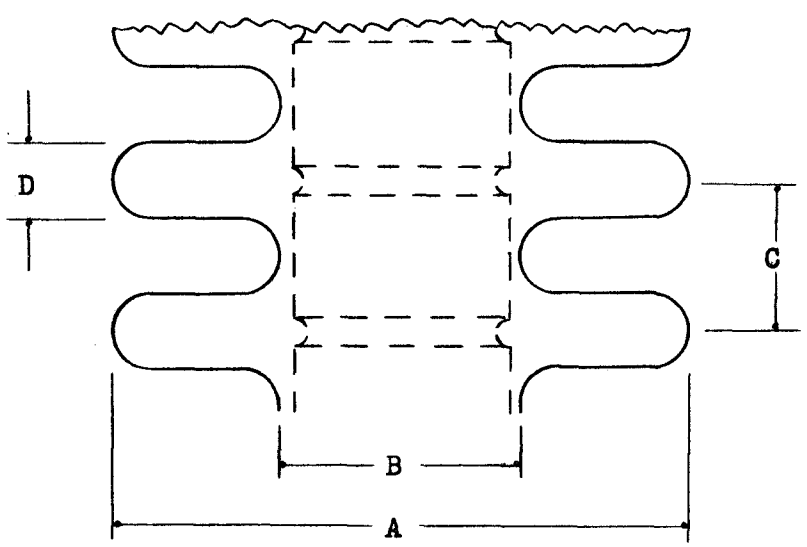

Figure 7: Dimensions as tabulated in Table I.

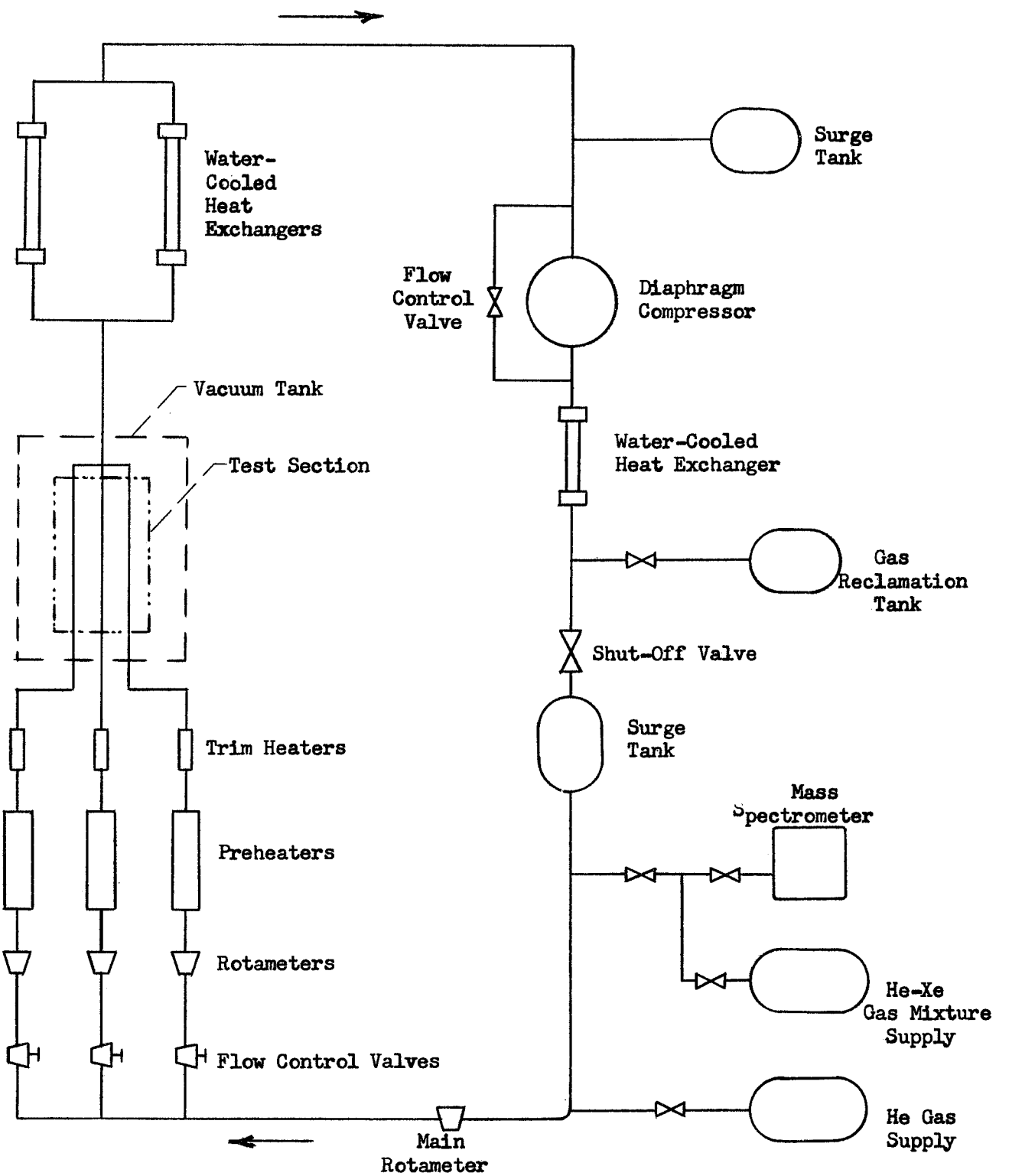

Figure 8: Schematic Diagram of Receiver Tube Test Gas Loop.

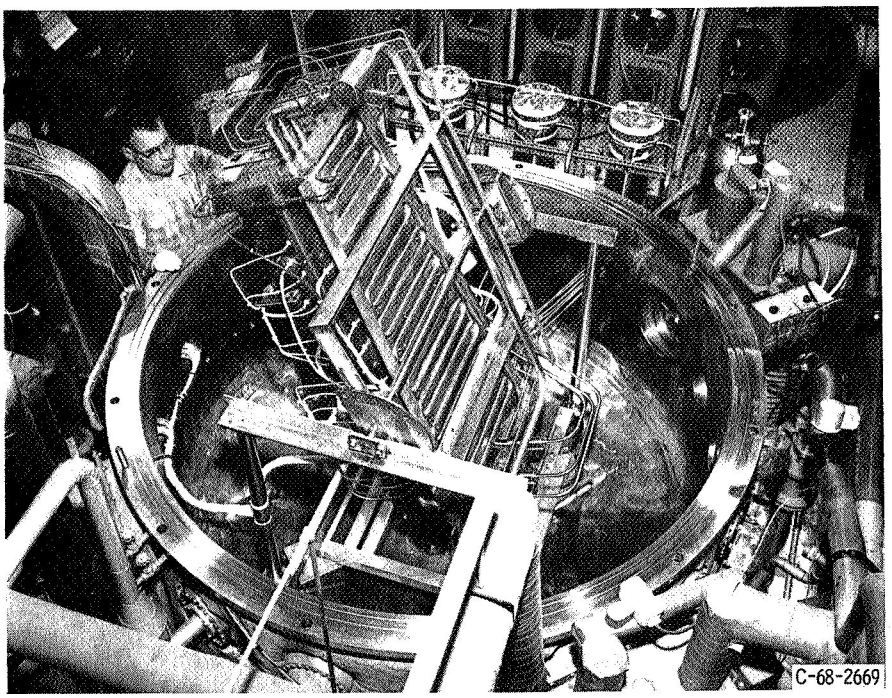

Figure 9. - 3-Tube section in vacuum tank.

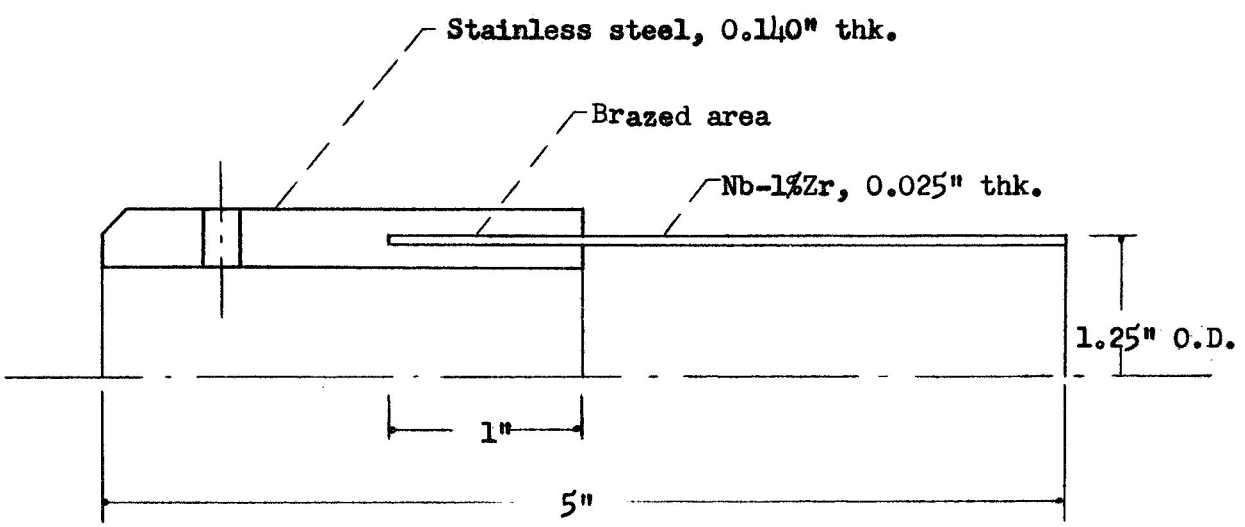

Figure 10: Cross-section of columbium-1% zirconium and stainless steel bi-metallic joint

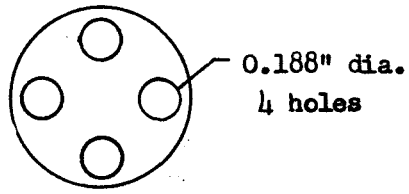

Detail A - 2 discs

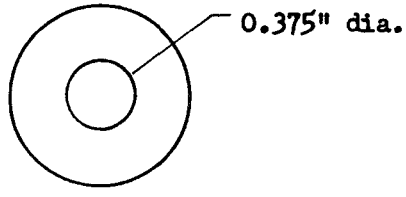

Detail B - 2 discs

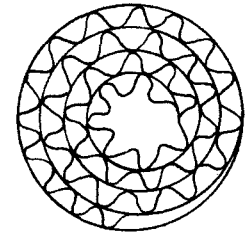

Detail C

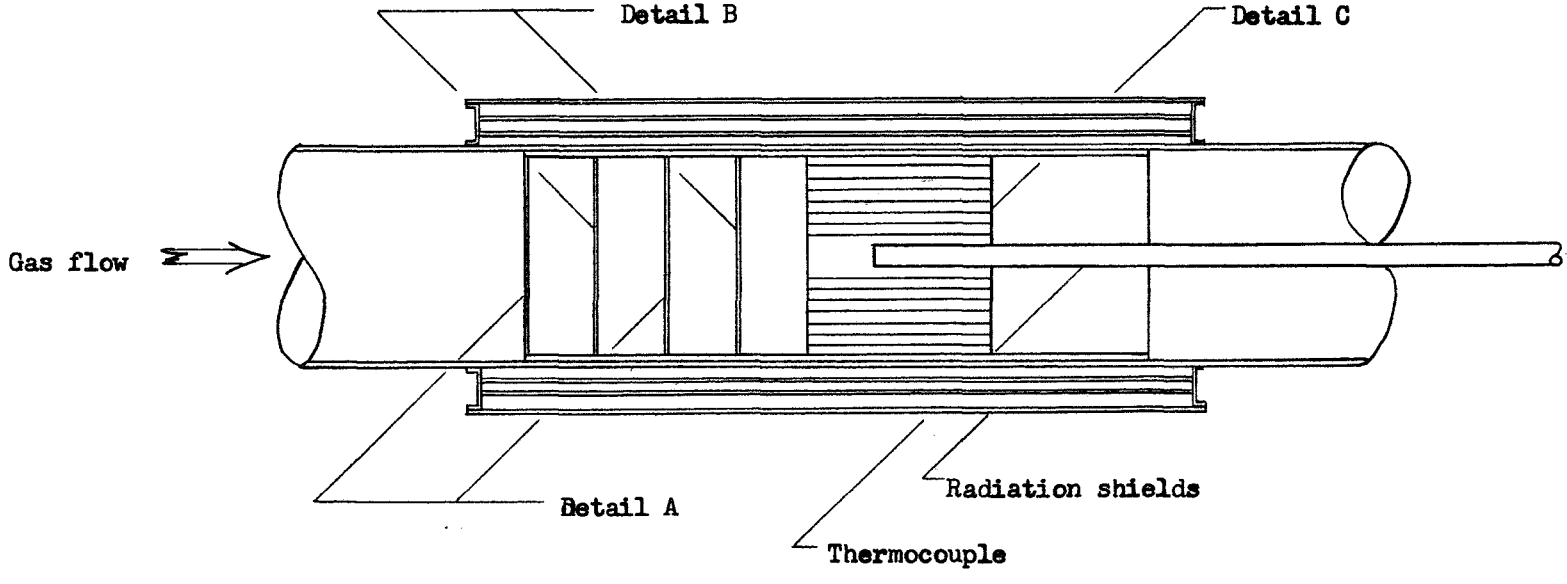

Figure 11: Gas temperature measuring section

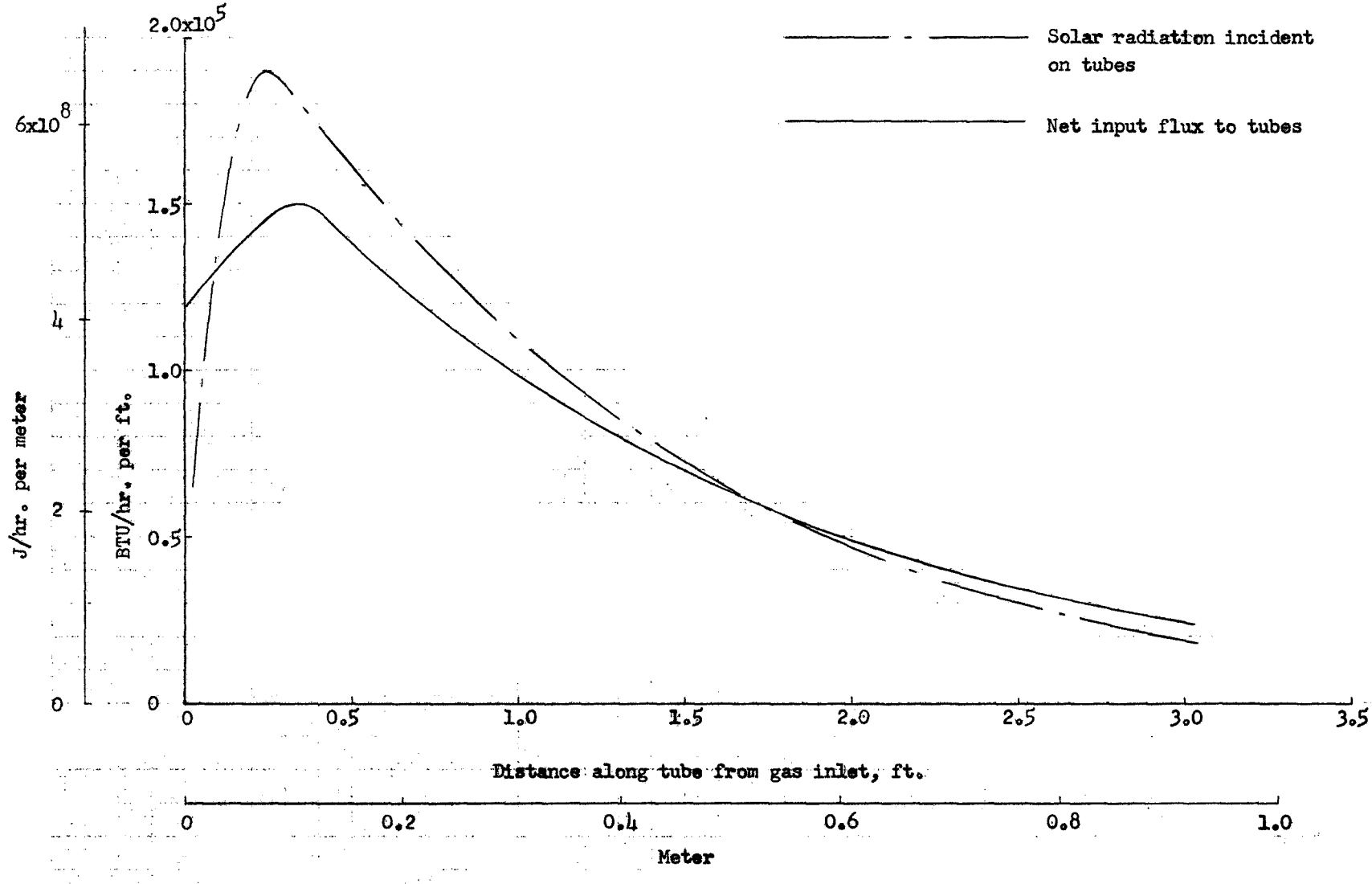

Figure 12: Flux distributions along gas tube length.

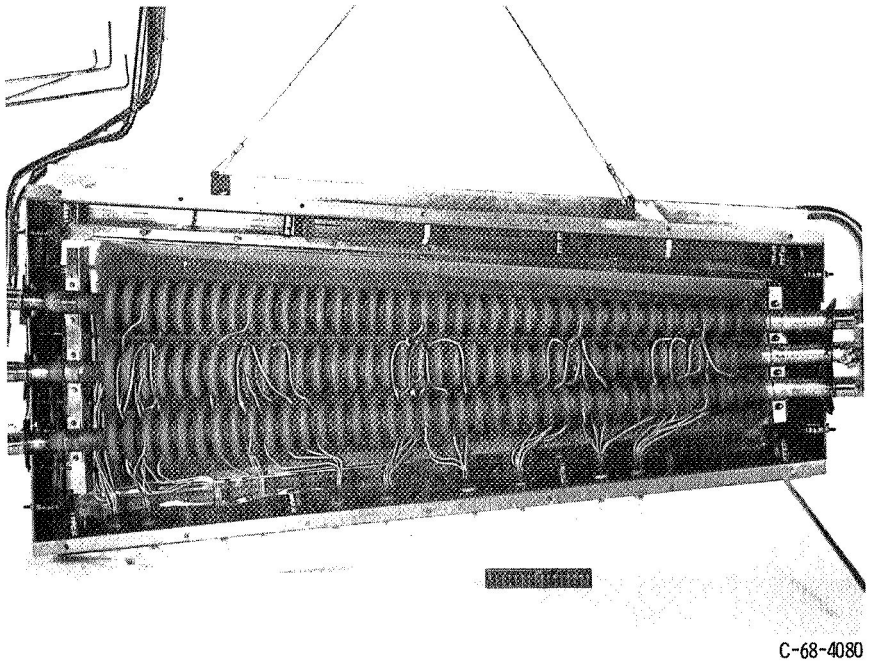

C-68-4080

Figure 13. - Iron titanate coated tubes after short-term test.

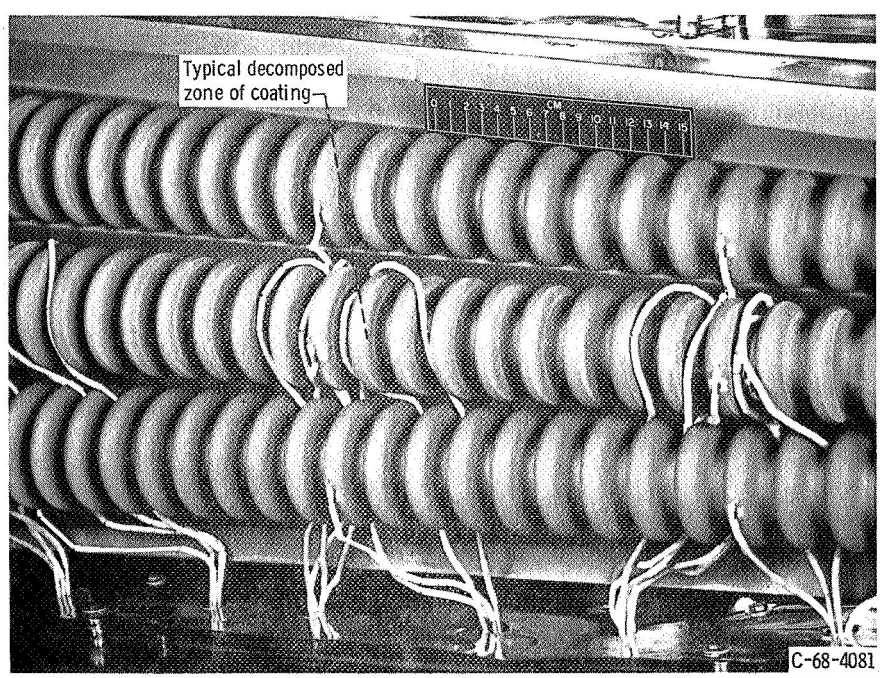

C-68-4081

Figure 14. - Close-up of middle region of iron titanate coated receiver tubes.

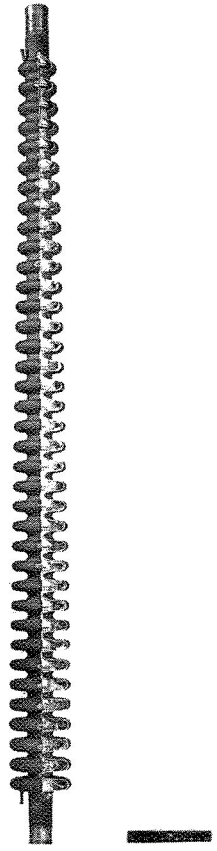

C-69-3922

Figure 15(a). - Cutaway of iron titanate coated tube showing lithium fluoride distribution on heater (180°) side.

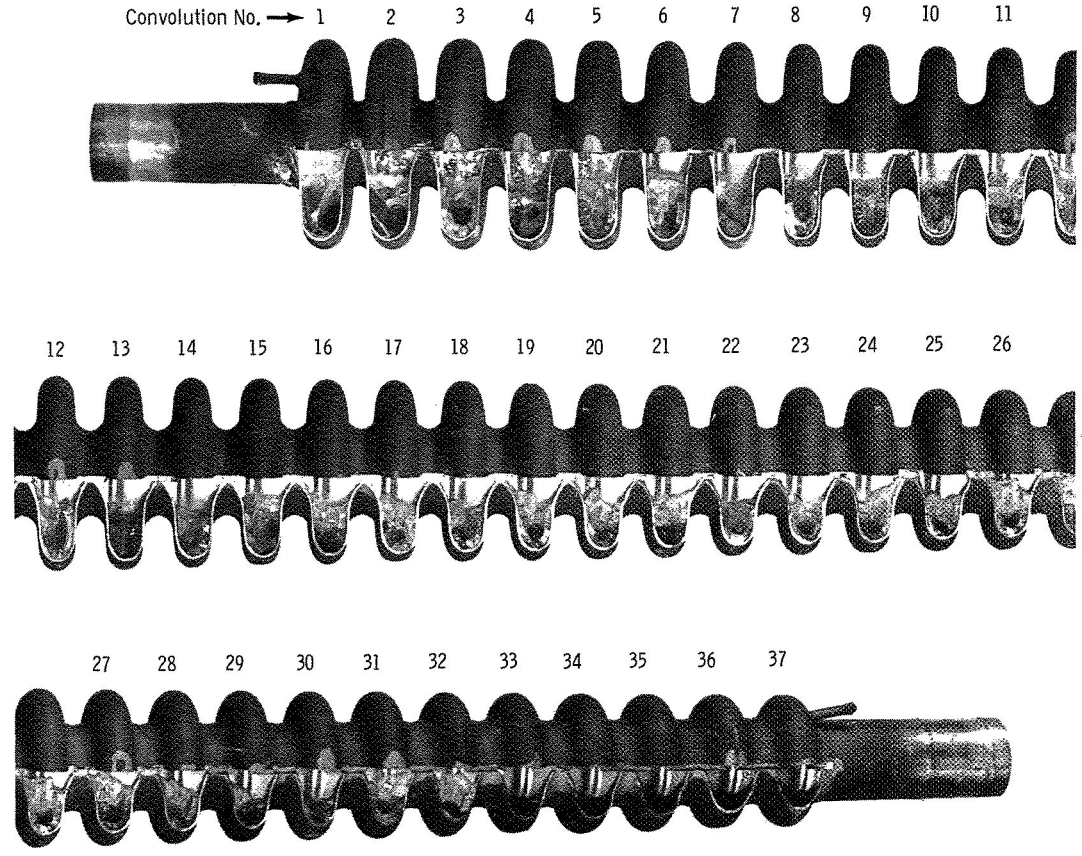

Figure 15(b). - Enlargement of receiver tube showing lithium fluoride distribution on heater (180°) side.

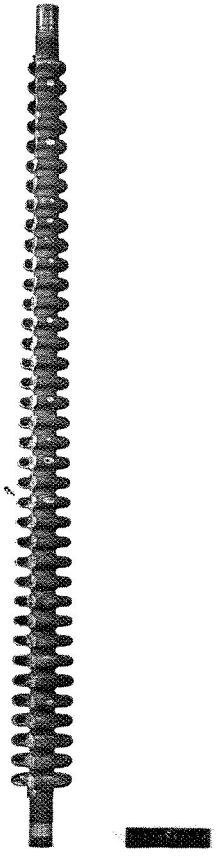

C-69-3923

Figure 16(a). - Cutaway of iron titanate coated tube showing lithium fluoride distribution on side opposite that of heater (0°).

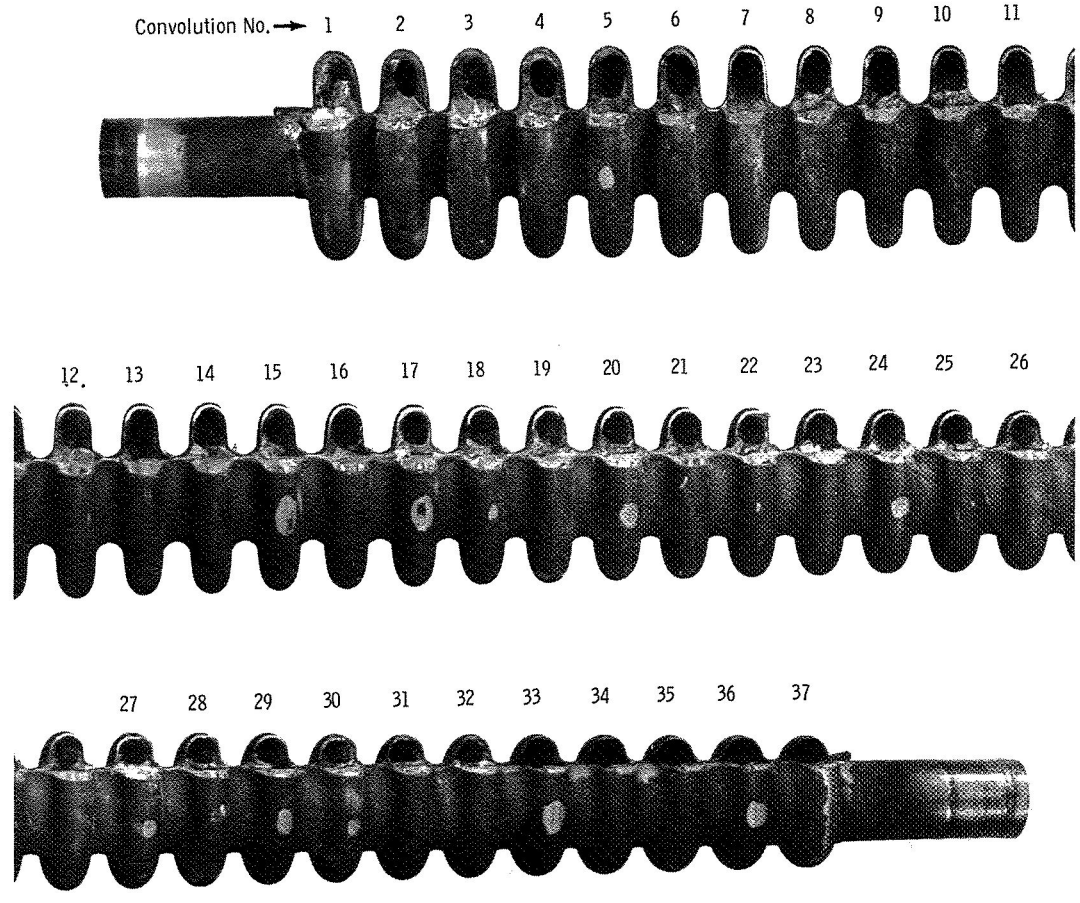

Figure 16(b). - Enlargement of receiver tube showing lithium fluoride distribution on side opposite that of heater (0°).

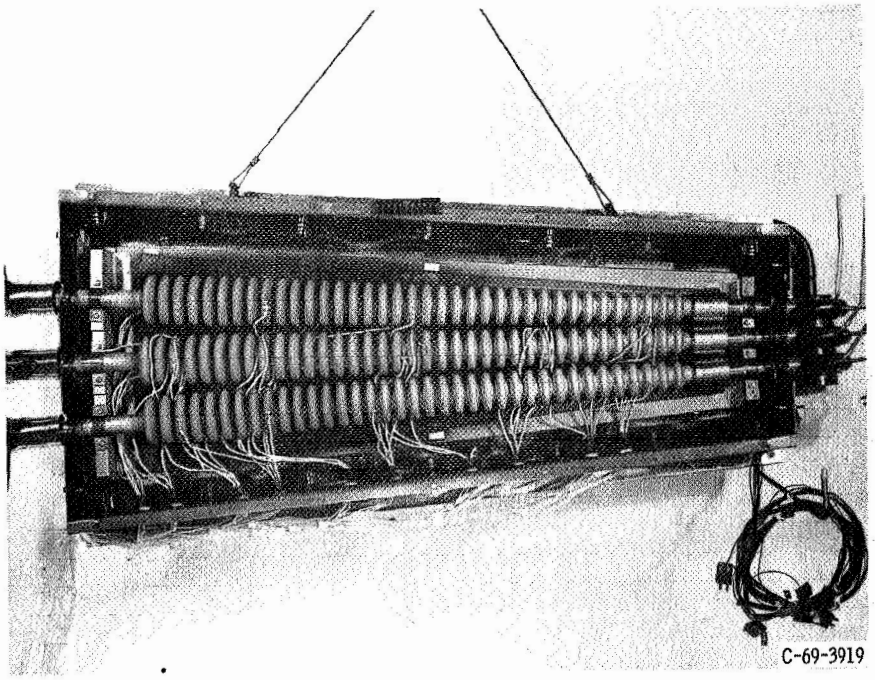

Figure 17. - Grit-blasted tubes in test section after 2002-hour test.

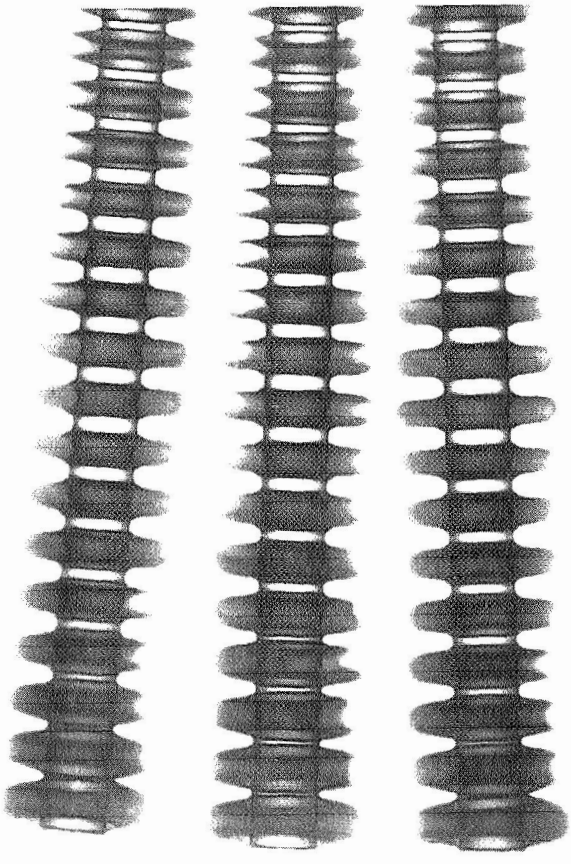

Figure 18. - Radiograph of tubes in inlet region after 2002-hour test.

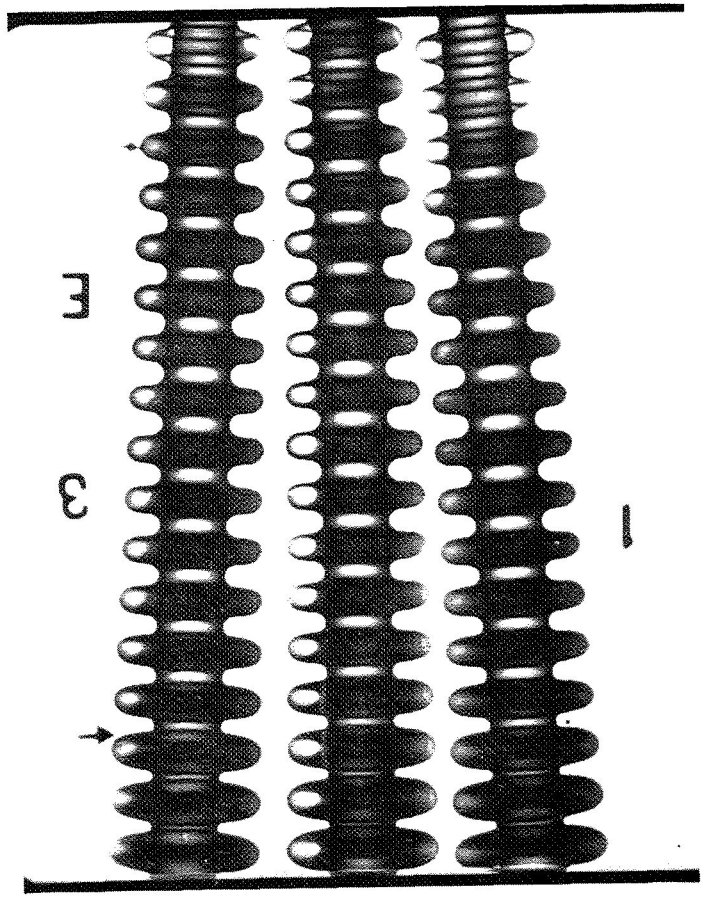

Figure 19. - Radiograph of tubes in mid-region after 2002-hour test.

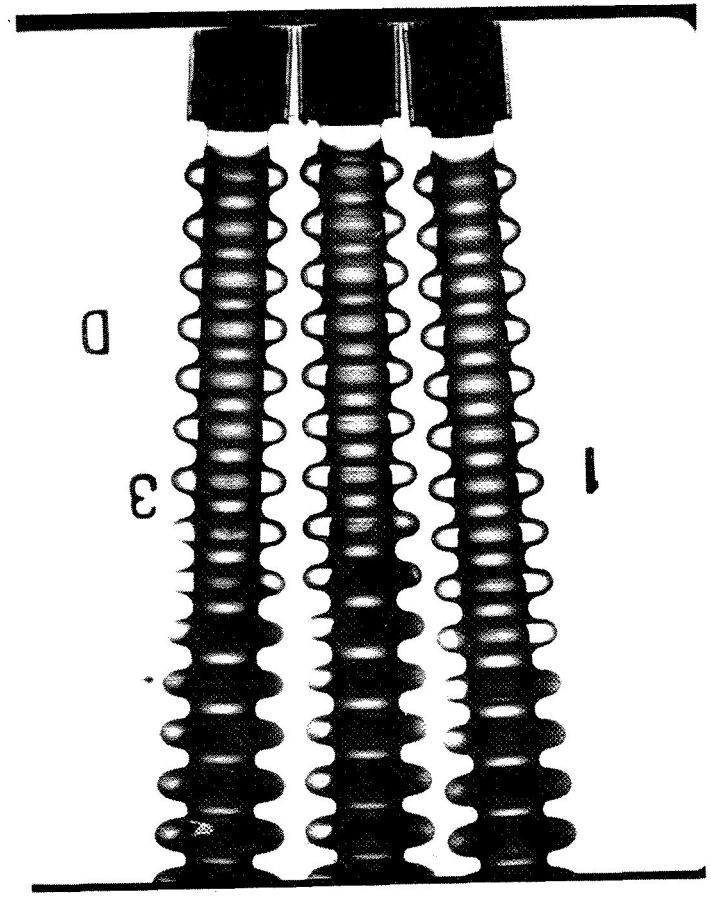

Figure 20. - Radiograph of tubes in exit region after 2002-hour test.

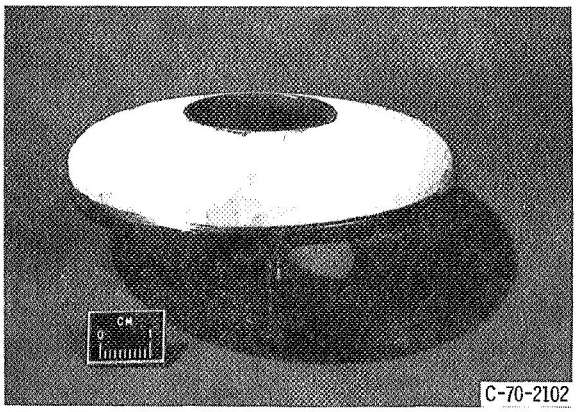

Figure 21. - Cutaway of first convolution showing fullness of LiF.

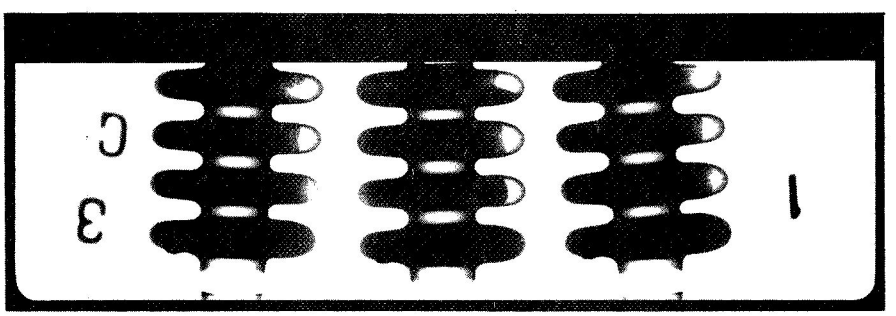

Figure 22. - Close-up radiograph of the first four convolutions from the inlet.

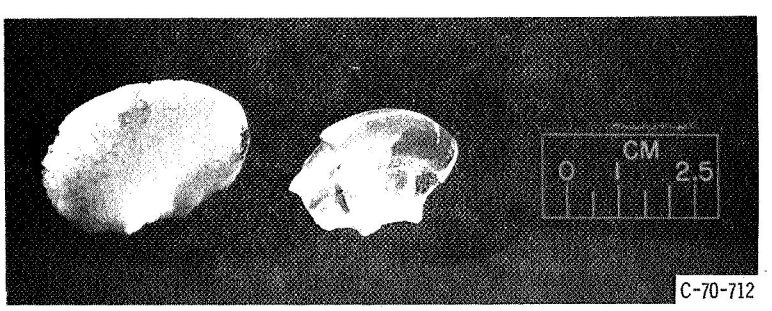

Figure 23. - Comparison of frozen LiF from convolution No. 4 (left) and convolution No. 18 (right).

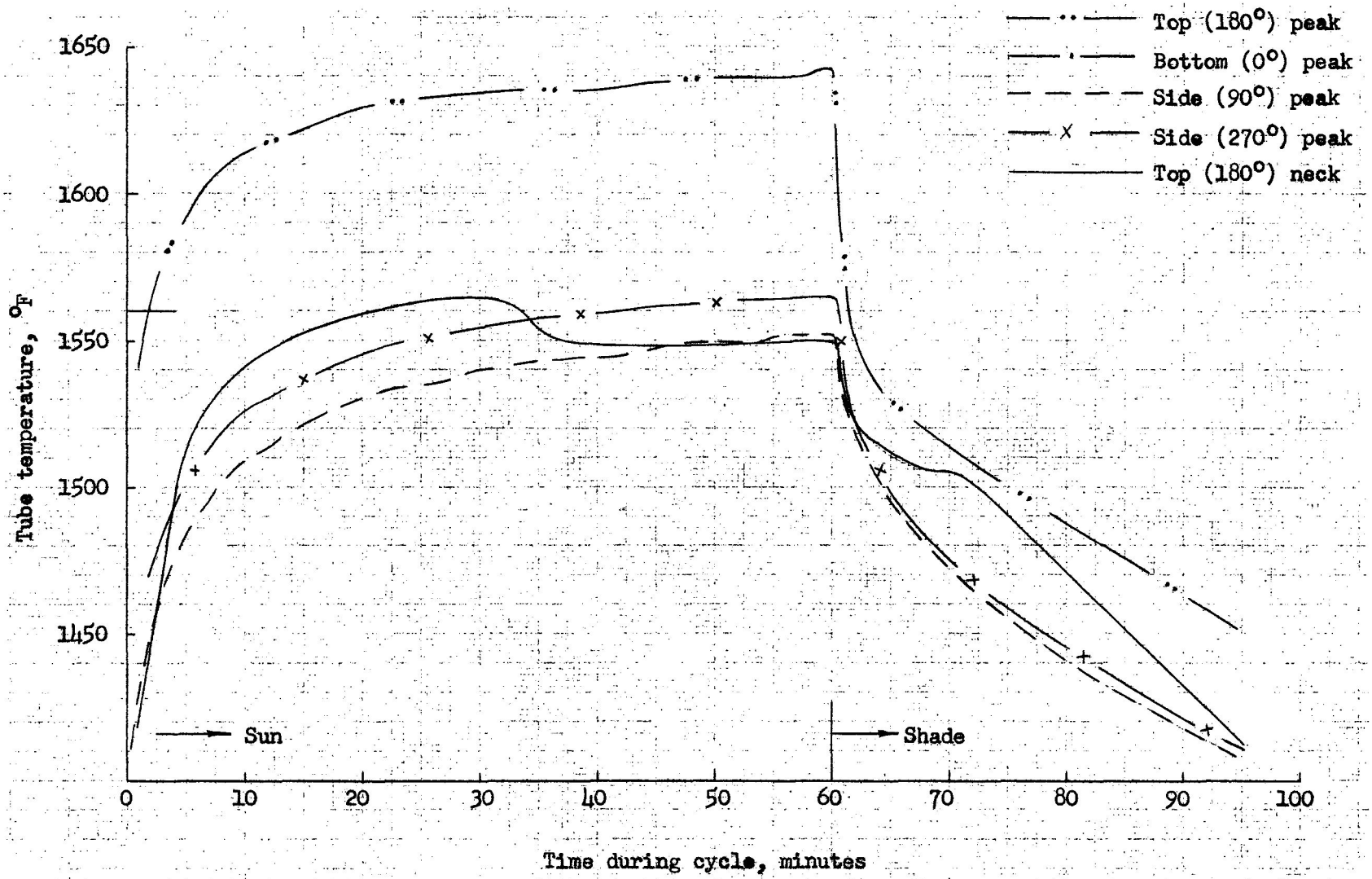

Figure 24: Convolution no. 3 temperature during 1240th cycle.

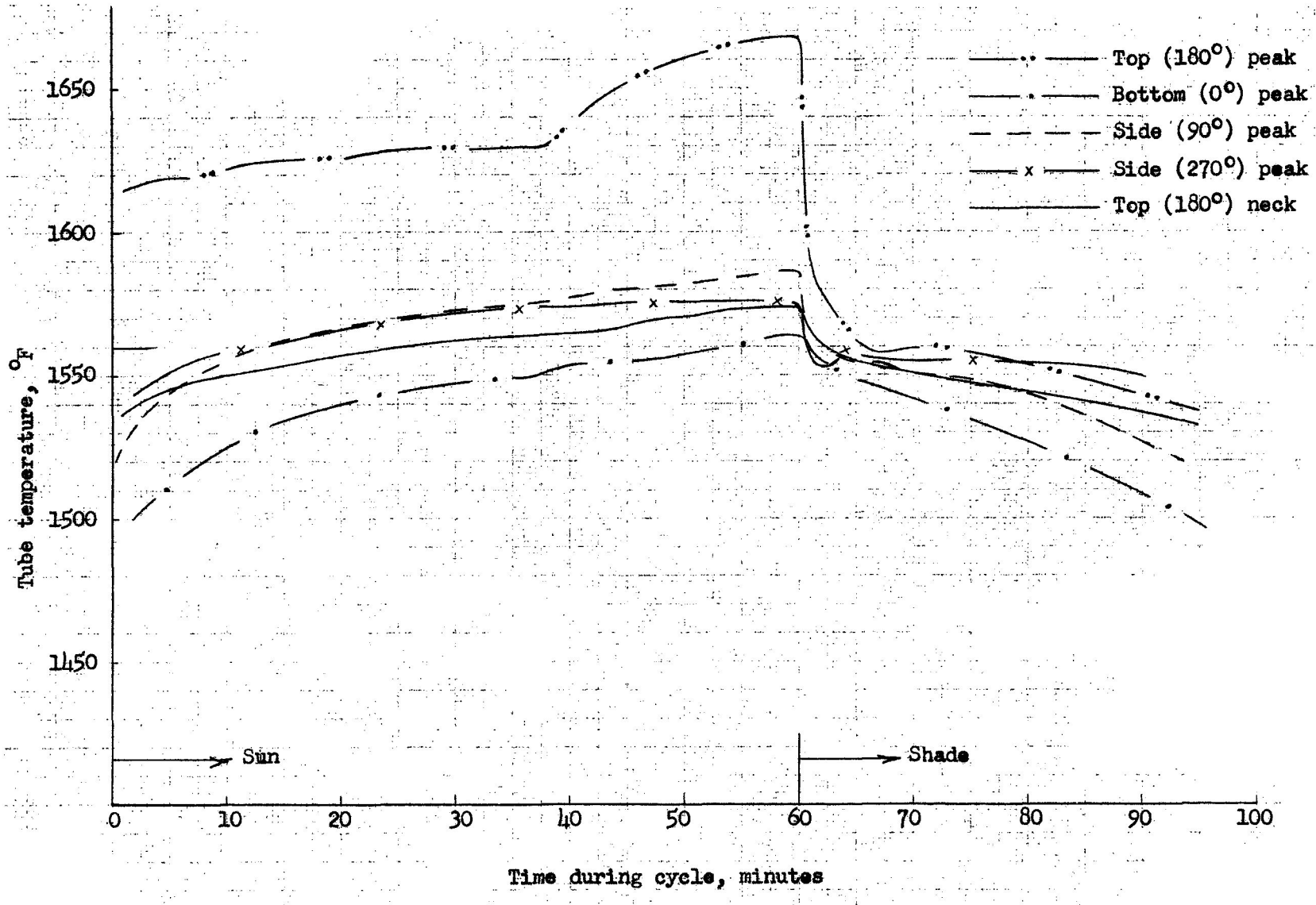

Figure 25: Convolution no. 9 temperature during 1240th cycle.

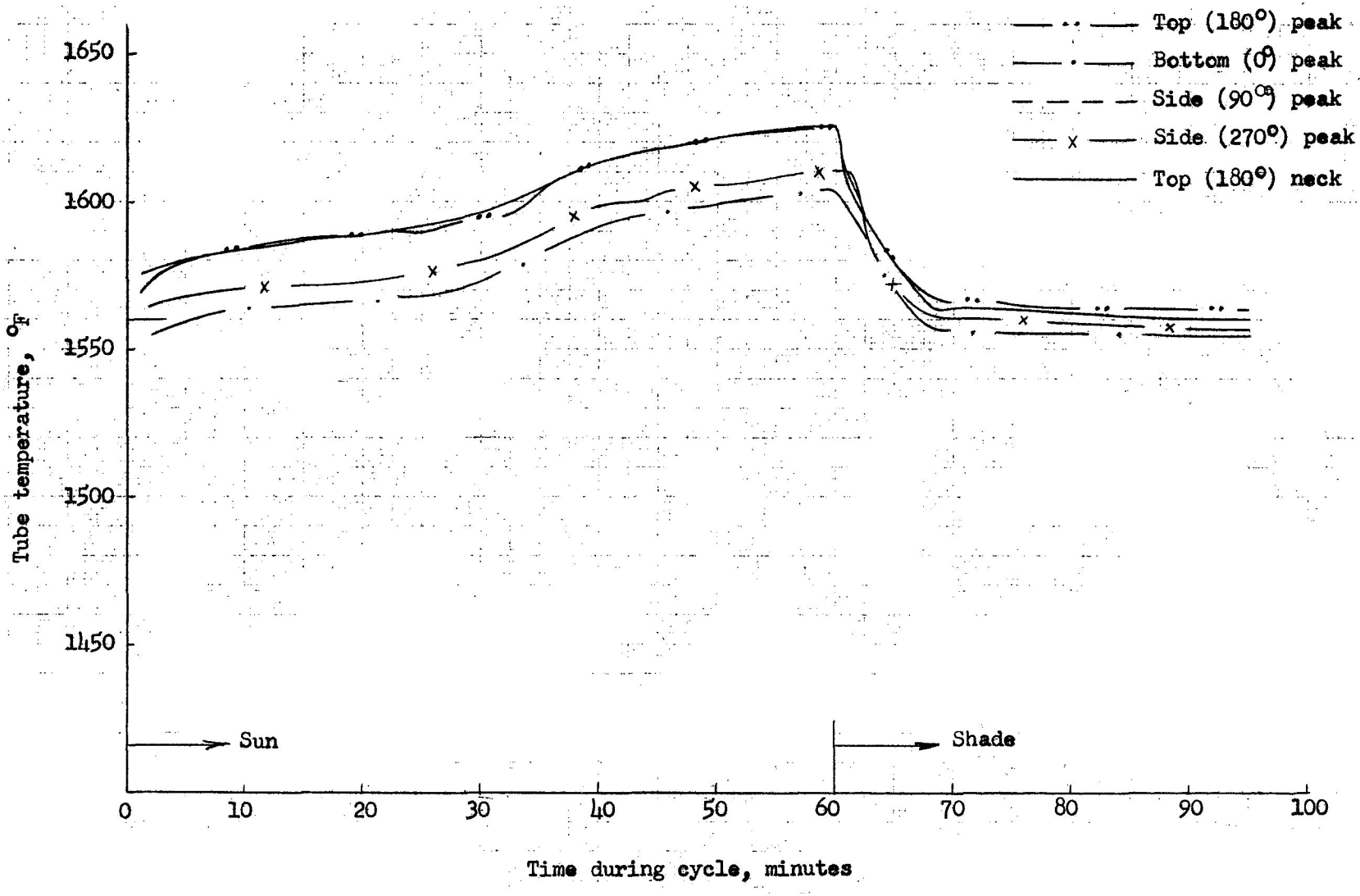

Figure 26: Convolution no. 19 temperature during 1240th cycle.

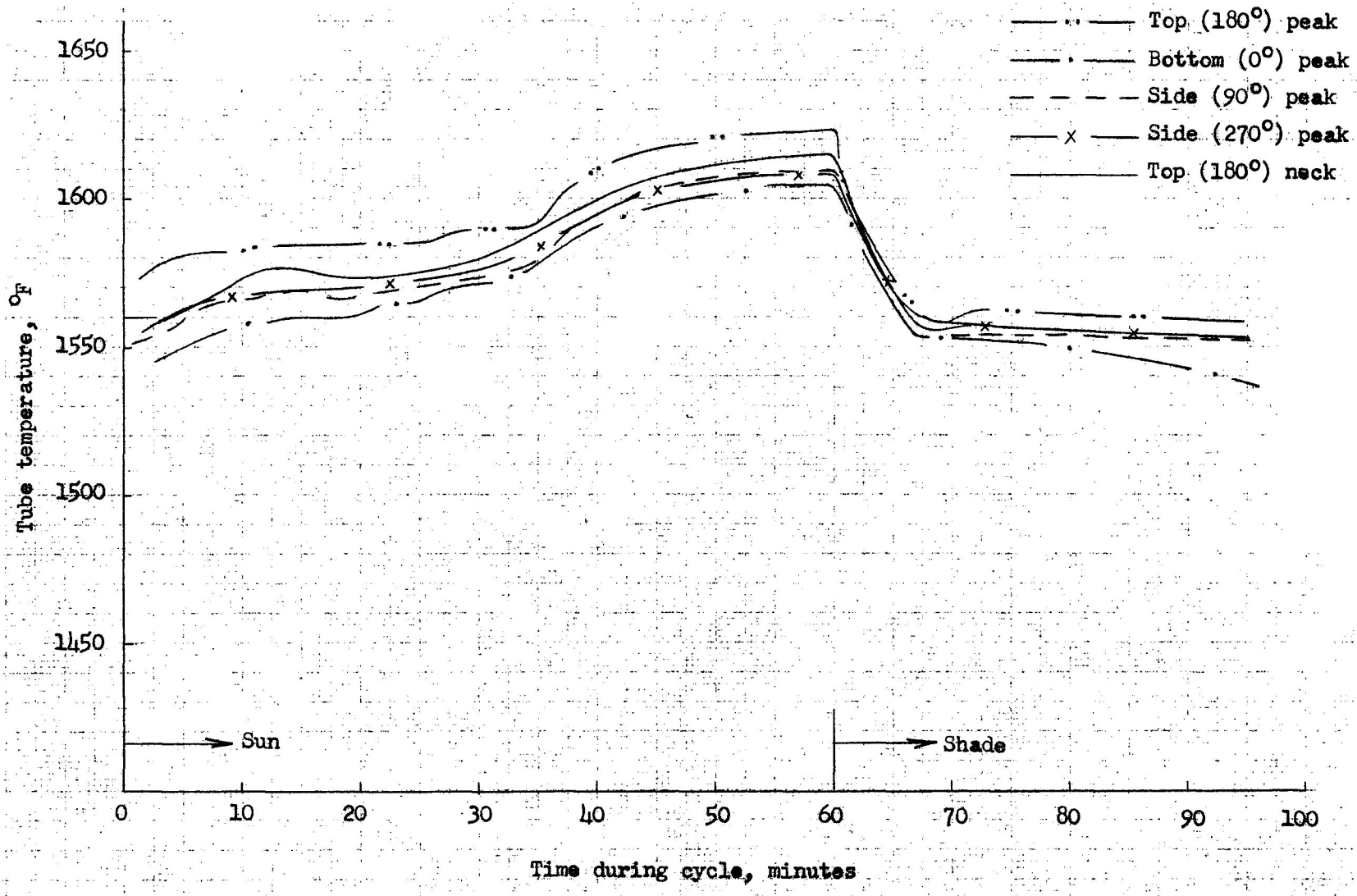

Figure 27: Convolution no. 28 temperature during 1240th cycle.

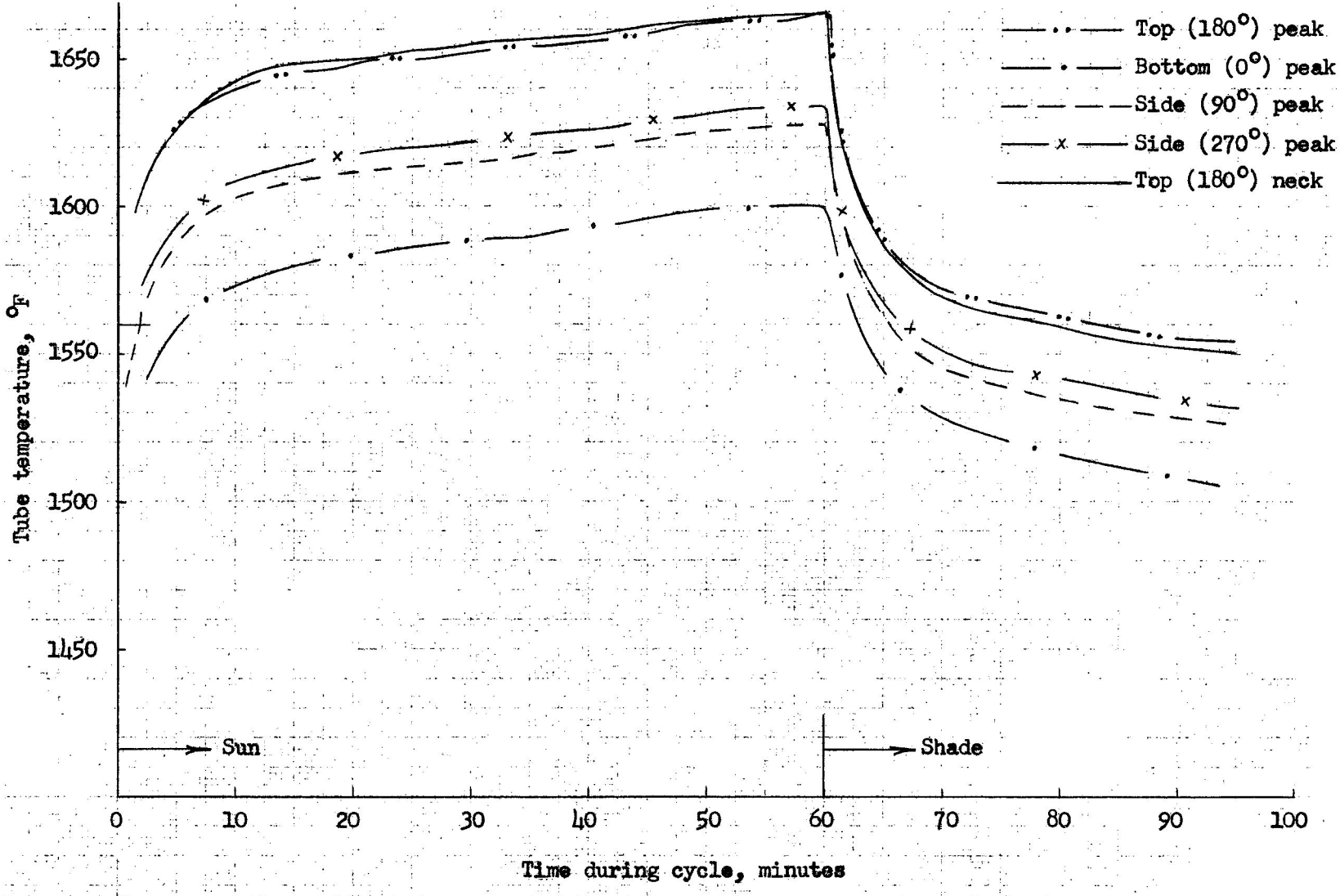

Figure 28: Convolution no. 35 temperature during 1240th cycle.

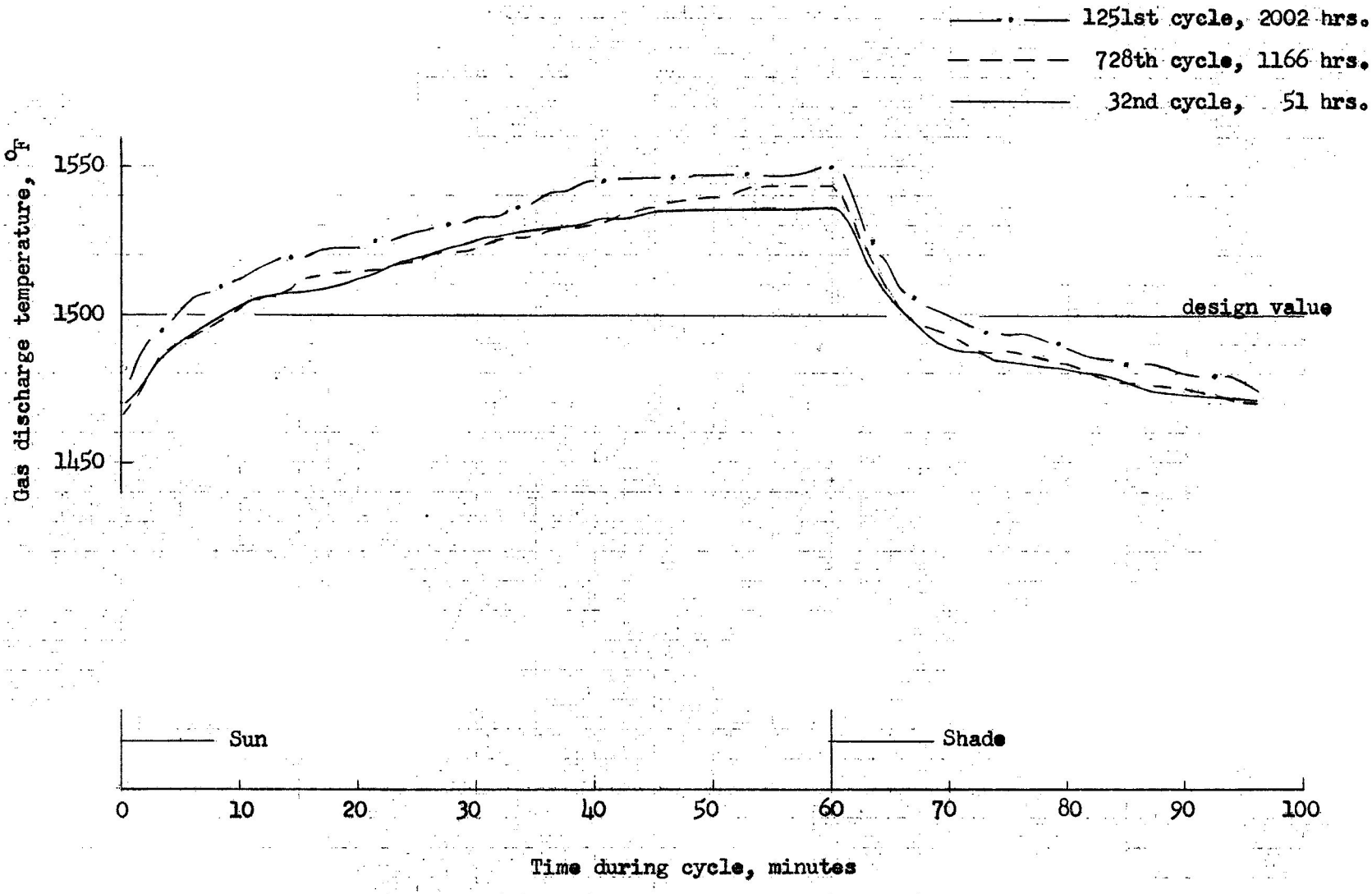

Figure 29: Gas discharge temperature during cycles.

Figure 30. - Photo (X600) of deposit on columbium.

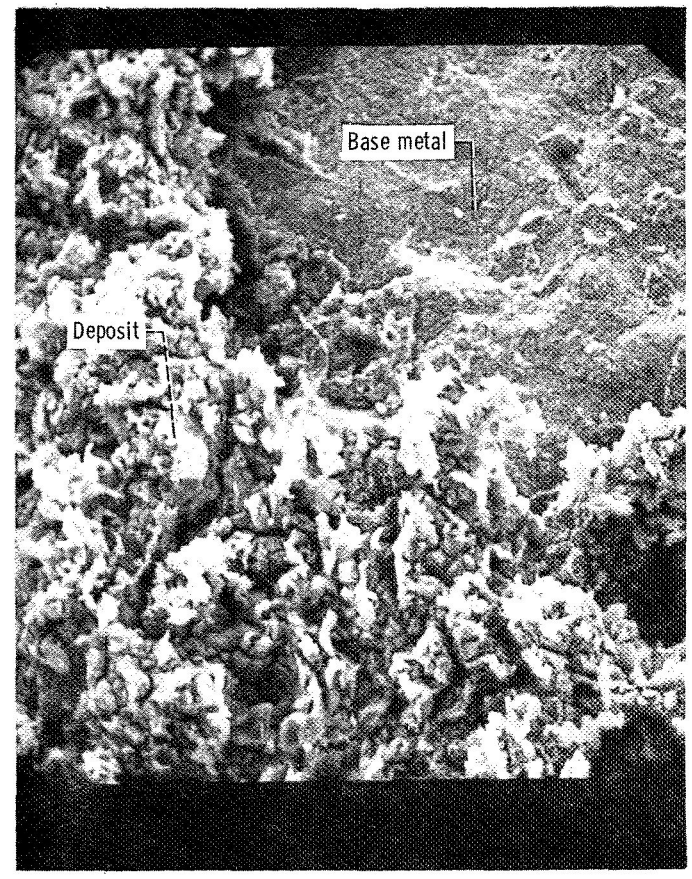

Figure 31. - Contrast between deposit and base material (X600).

E-6511

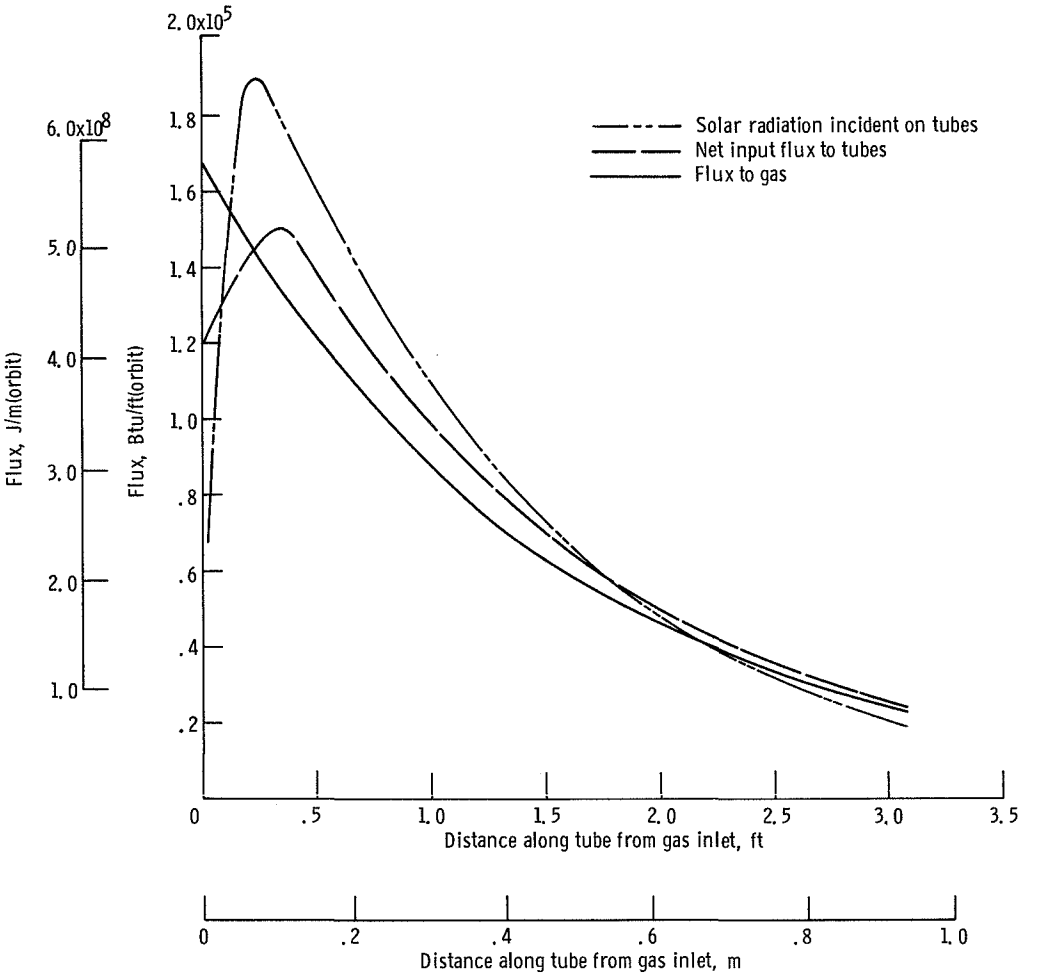

Figure 32. - Flux distributions along gas tube length for 60-minute sun period, 36-minute shade period orbit.